Transportation Research Part B 203 (2026) 103352

Contents lists available at ScienceDirect

Transportation Research Part B

journal homepage: www.elsevier.com/locate/trb

Leveraging cooperative connected automated vehicles for mixed traffic safety

Chenguang Zhao [a], Tamas G. Molnar [b], Huan Yu [a,*]

[a] Thrust of Intelligent Transportation, The Hong Kong University of Science and Technology (Guangzhou), Nansha, 511400, Guangzhou, Guangdong, China

[b] Department of Mechanical Engineering, Wichita State University, 67260, Wichita, KS, USA

ARTICLE INFO

Keywords:
Connected and automated vehicle
Mixed traffic
Stability analysis
Traffic safety

ABSTRACT

The introduction of connected and automated vehicles (CAVs) is expected to reduce congestion, enhance safety, and improve traffic efficiency. Numerous research studies have focused on controlling pure CAV platoons in fully connected automated traffic, as well as single or multiple CAVs in mixed traffic with human-driven vehicles (HVs). While cruise control designs for CAVs have been proposed to stabilize car-following dynamics, few studies have addressed their impact on safety, particularly the trade-offs between stability and safety. In this paper, we study how cooperative control strategies for CAVs can be designed to enhance the safety and stability of mixed traffic, under various levels of connectivity and automation. Considering mixed traffic where a pair of CAVs travels amongst HVs, we design cruise control strategies for the head and the tail CAVs to stabilize traffic via cooperation and, possibly, by also leveraging connectivity with HVs in-between. We introduce the definition of CAV safety, HV safety, and platoon safety, and investigate the real-time safety impact of the CAV controllers using control barrier functions (CBFs). Safety-critical control strategies are then derived by incorporating CBF safety constraints for online computation. Both theoretical and extensive numerical analysis have been conducted to explore the effect of CAV cooperation and HV connectivity on the stability and safety of mixed traffic. The cooperative strategy for CAV control improves stability, and potential safety issues are successfully resolved with the proposed safety-critical design. Moreover, connecting CAVs with the HVs between them offers additional benefits: if HVs are connected to the tail CAV, traffic stability is further improved compared to when they are connected only to the head CAV; whereas if HVs are connected to the head CAV, their safety can be enhanced.

1. Introduction

The integration of automation and connectivity in intelligent vehicles has been envisioned to improve road transportation efficiency, fuel consumption, and driving safety. Many studies have focused on the control of connected and automated vehicles (CAVs) to explore their potential for improving traffic under different penetration rates ranging from a single automated vehicle to fully connected automated traffic systems Ding et al. (2020), Seyedeh et al. (2021). Before fully automated and connected traffic becomes reality, there will still be an inevitable transition period of mixed traffic systems, which are characterized by frequent interactions between CAVs and conventional human-driven vehicles (HVs). In mixed traffic, the cooperative control of CAVs remains a significant

* Corresponding author.
E-mail address: huanyu@hkust-gz.edu.cn (H. Yu).

https://doi.org/10.1016/j.trb.2025.103352
Received 22 May 2024; Received in revised form 21 October 2024; Accepted 29 October 2025

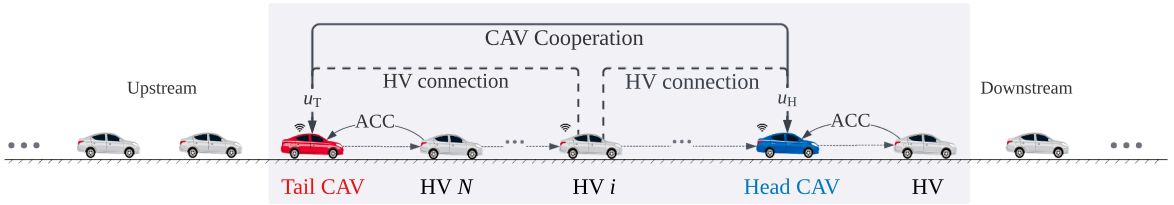

Fig. 1. Safety-critical stabilization of mixed traffic via a pair of CAVs. The head CAV follows a downstream head HV and leads N following HVs, while the tail CAV follows the last HV in this vehicle platoon. We design controllers for the CAVs to alleviate congestion and also maintain formal safety guarantees considering the mixed vehicle platoon shaded in grey.

challenge. Especially, the safety impact of cooperative CAV control strategies on surrounding vehicles needs to be addressed. In this paper, we investigate this problem for a mixed vehicle platoon that includes a pair of cooperative CAVs traveling amongst (possibly connected) HVs as shown in Fig. 1. We explore in detail how coordination between CAVs and feedback from surrounding connected HVs influence the effectiveness of control strategies in achieving safety and smoothness of mixed traffic, under various penetrations of connectivity and automation.

1.1. Stability and safety by controlling a single CAV

Automated vehicles have the potential to stabilize traffic by generating smooth driving motions in car-following scenarios. Speed perturbations are attenuated in the process of propagating from the leader vehicle to the followers Giammarino et al. (2020), Stern et al. (2018), Yu et al. (2018), Zhou et al. (2023a). To achieve smooth motion, controllers have been designed for automated vehicles under different penetration rates of CAVs in traffic and different accessibility of surrounding traffic information. In adaptive cruise control (ACC), the automated vehicle is controlled based on data measured via onboard sensors, which include its speed, the preceding vehicle's speed, and the gap (distance) ahead Gunter et al. (2020). The performance of automated vehicles can be further improved by using additional information from vehicle-to-vehicle (V2V) connectivity. CAVs equipped with communication devices may obtain data from downstream or upstream connected HVs that are also equipped with communication devices. This is leveraged by connected cruise control Orosz (2016), which enables CAVs to respond not only to the immediate preceding vehicle but also to other connected HVs downstream. Field experiments in Ge et al. (2018) have shown that this additional information from the downstream traffic helps the CAV to drive smoother compared to ACC-only vehicles, which improves traffic stability. Connectivity between the CAV and upstream HVs can also improve traffic stability by the notion of leading cruise control Wang et al. (2022). As the CAV responds to connected HVs upstream, the stability of the upstream traffic is further enhanced.

In order to implement controllers for CAVs in practice, safety must be guaranteed Ye and Yamamoto (2019). In this paper, we focus on longitudinal control, and thus safety refers to eliminating the risk of rear-end collisions. Longitudinal controller design exhibits a trade-off between stability and safety Li (2022). For example, when the vehicle ahead of the CAV decelerates, a smaller deceleration of the CAV leads to smoother traffic but also a higher risk of collisions. To ensure safety for the controlled dynamical systems, representative control techniques include model predictive control (MPC) Bai et al. (2022a), reachability analysis Althoff and Dolan (2014), Zhao et al. (2022), and control barrier functions (CBFs) Ames et al. (2014), Xiao et al. (2021). MPC typically minimizes stability-related indices such as speed perturbation or energy consumption while safety is usually considered as a constraint over the prediction horizon. CBFs, on the other hand, directly give a constraint on the controller to guarantee safety based on the current system state. Therefore, CBFs avoid the computation burden from the prediction of future dynamics which could possibly be inaccurate. Furthermore, CBFs can be integrated with pre-designed nominal controllers. In particular, safety-critical controllers have been developed that minimize the deviation from the nominal controller while satisfying the CBF safety constraint Ames et al. (2019, 2014). In this approach, CBF acts as a safety filter that only alters the nominal controller when the system is in danger of violating safety.

Many recent results have employed CBFs to enhance traffic safety. CBFs have been integrated with adaptive cruise control in Ames et al. (2014) to ensure the safety of automated vehicles. CBF-based safety filters have also been developed for connected cruise control in Chaozhe et al. (2018), Molnar et al. (2023) to avoid collisions for a CAV that is connected to HVs downstream. Furthermore, CBF constraints have been designed for safety-critical traffic control in Zhao et al. (2023) to ensure safety for both the CAV and following HVs when the CAV is connected to HVs upstream. In this paper, we develop a novel CBF framework to evaluate the stability and safety impact of cooperative CAV control strategies on the upstream and downstream traffic. More importantly, we analyze the trade-offs between stability and safety, and in particular, how connectivity of HVs, ACC and cooperation between CAVs play a role in it. The safety-critical control designs proposed in this paper achieve stability and safety simultaneously.

1.2. Cooperative control of multiple CAVs

Besides analyzing the effect of a single automated vehicle on traffic, research has also shown that communication and coordination between multiple CAVs may further improve the overall performance of the traffic system Do et al. (2019), Garg and Bouroche (2023), Papadoulis et al. (2019), Talebpour et al. (2016). Cooperative controllers have been considered for various traffic scenarios,

such as cooperative cruise control and platooning Johansson et al. (2023), Wang et al. (2024), cooperative merging at highway on-ramps Rios-Torres and Malikopoulos (2016), Wang et al. (2018), cooperative lane changing Zhang et al. (2022), Zheng et al. (2019), and cooperative eco-driving at signalized and unsignalized intersections Bai et al. (2022b), Chen et al. (2023), Han et al. (2020). In longitudinal control, an important case is when multiple adjacent CAVs follow each other and form a CAV platoon. Related research has revealed the positive improvement brought by such CAV platoons on traffic throughput Jin et al. (2020), Zhou and Zhu (2021), energy Kim et al. (2021), stability Zhou et al. (2023b), mobility Liu et al. (2020), and safety Yi et al. (2020).

To unleash the potential of CAV platoons, however, it is crucial to design controllers that effectively coordinate CAVs. A prevailing approach is cooperative adaptive cruise control (CACC), which is an extension of ACC Dai et al. (2022), Dey et al. (2015). Compared with ACC, CACC allows the CAVs within the platoon to have a smaller gap, and improves traffic stability, efficiency, and throughput Brunner et al. (2022). As for safety, CACC with well-designed controller gains also achieves collision-free driving for CAVs Bekiaris-Liberis (2023).

Despite their benefits, CAV platoons may be difficult to implement in practice, since full penetration of automation and connectivity is required within the platoon. As opposed, the penetration rate of CAVs is typically low in current traffic conditions. With low penetration, a more common scenario is mixed vehicle platoons consisting of both CAVs and HVs as shown in Fig. 1. To coordinate CAVs that are separated by HVs, controllers have been designed via multiple tools, such as MPC Gong and Du (2018), Qiu and Du (2023), feedback control Guo et al. (2023), and reinforcement learning Shi et al. (2021). These studies have shown that, compared with controlling the two CAVs separately, cooperative strategies further improve mixed traffic efficiency and stability. For safety, MPC-related controllers Gong and Du (2018), Qiu and Du (2023) include CAV safety conditions as constraints in the optimization problem, while other controllers fail to provide safety guarantees.

The above research considers the case where HVs are not connected, and thus, feedback about their motion may not be available to the CAVs. Yet, as has been discussed above for the control of a single CAV, the traffic efficiency Vaio et al. (2019), Orosz (2016), Shladover et al. (2012), Wang et al. (2022) and safety Zhao et al. (2023) can be further improved via connecting HVs to CAVs. For the coordination of multiple CAVs, it remains unexplored how additional connectivity to HVs affects traffic stability and safety. On the other hand, scarce studies have focused on designing CAV control strategies to guarantee the safety of surrounding HVs in mixed traffic, which will be discussed in our paper. We design safety-critical controllers for a cooperating pair of CAVs that stabilizes the mixed traffic while considering both CAV and HV safety, and we analyze how the connection of HVs can be leveraged to improve the stability and safety of the system.

1.3. Contribution

In this paper, we consider a mixed vehicle platoon shown in Fig. 1 that contains HVs enclosed by two CAVs. The CAVs are equipped with communication devices and thus can obtain information about each other's state, while some of the middle HVs may also have the ability for V2V communication. By leveraging the information from connectivity, we design controllers for the pair of CAVs to stabilize the motion of the mixed vehicle platoon while maintaining safety of the CAVs and the middle HVs. We first design a nominal stabilizing controller consisting of three parts: adaptive cruise control, feedback of middle HV states (if there are connected HVs), and CAV coordination. Then, we discuss safety against rear-end collisions, and propose safety notions considering the CAVs, the middle HVs, and the overall platoon. We perform safety analysis for the nominal controller, and then design CBF-based safety filters to guarantee safety for CAVs, HVs, and the overall platoon, respectively. Finally, we conduct numerous simulations to validate our safety-critical cooperative CAV controllers and analyze their impact on stability and safety, sensitivity to the penetration rate of CAVs, and robustness to uncertain human driver behaviors.

The main contribution of this paper lies in proposing a methodological cooperative control framework for pairing CAVs to guarantee the safety of mixed traffic, including CAVs safety, HVs safety and platoon safety. In particular, we analyze how the connection of HVs affects stability and safety, and show that if an HV is equipped with V2V communication devices, the CAVs can simultaneously enhance the safety of the HV and the smoothness of the following traffic. In our previous works Guo et al. (2023), Zhao et al. (2024, 2023), we obtained preliminary results on using CBFs to enhance traffic safety. The impact of cooperative strategies on the trade-offs between stability and safety has not yet been explored, especially for mixed traffic. More importantly, we leverage the connection of HVs to improve the safety of mixed traffic systems by establishing CBF safety constraints for the pair of CAVs, HVs, and the platoon. The practical impact of our proposed control strategies is extensively studied across various safety-critical scenarios, considering different penetration rates of CAVs and accounting for uncertain human driver behaviors.

The remainder of this paper is organized as follows. We formulate the model of the mixed vehicle platoon in Section 2. We establish a nominal controller and address stability in Section 3. In Section 4, we conduct safety impact analysis and propose cooperative control designs that guarantee the safety of the CAVs, HVs, and the platoon based on CBFs. We conduct numerical simulations in Section 5 to validate the designed controller. We analyze controller performance from various aspects in Section 6, including controller parameter selection and robust stability and safety against unmodeled HV dynamics.

2. Problem formulation

We consider a mixed vehicle platoon, shown in Fig. 1, that includes two CAVs and N HVs between them. The head CAV (H-CAV) follows an HV that leads the vehicle platoon and may cause velocity disturbance, while the tail CAV (T-CAV) follows the last HV (HV-N) in the platoon. The two CAVs can measure their own gap, their own speed, and the speed of their preceding vehicle by

onboard sensors (such as radar, lidar, or camera). Furthermore, the head and tail CAVs share information about each other's real-time position and speed via V2V communication. The states of the middle HVs are available to the CAVs if they are equipped with communication devices (i.e., they are connected HVs). We will discuss how to design safe cooperative CAV control strategies from null connectivity to full connectivity of middle HVs. The considered vehicle chain can be viewed as one module in more complex mixed traffic systems. If there is a long vehicle chain with multiple CAVs, the whole vehicle chain can be split into several sub-chains, each having the structure as in Fig. 1 and being controlled by our proposed controller.

The state variable of the mixed traffic system $\mathbf{x}(t) \in \mathbb{R}^n$ with $n = 2N + 4$ is defined as:

$$\mathbf{x} = [\underbrace{s_{\mathrm{H}}, v_{\mathrm{H}}}_{\text{head CAV}}, \underbrace{s_1, v_1, \cdots, s_{\mathrm{N}}, v_{\mathrm{N}}}_{\text{HVs}}, \underbrace{s_{\mathrm{T}}, v_{\mathrm{T}}}_{\text{tail CAV}}]^\top \in \mathbb{R}^n, \tag{1}$$

with $s_{\mathrm{H}}(t) \in \mathbb{R}$ being the gap between the head CAV and its leader HV, $v_{\mathrm{H}}(t) \in \mathbb{R}$ being the speed of the head CAV, $s_{\mathrm{T}}(t) \in \mathbb{R}$ and $v_{\mathrm{T}}(t) \in \mathbb{R}$ being the gap and speed of the tail CAV, $s_i(t) \in \mathbb{R}$ and $v_i(t) \in \mathbb{R}$ being the gap and speed of HV-i with $i \in \{1, \ldots, N\}$. Meanwhile, the leader HV's speed $v_{\mathrm{d}}(t) \in \mathbb{R}$ is an external disturbance for the vehicle platoon. We design a control input $u_{\mathrm{H}}(t) \in \mathbb{R}$ for the head CAV and a control input $u_{\mathrm{T}}(t) \in \mathbb{R}$ for the tail CAV. The controller is represented by:

$$\mathbf{u} = \begin{bmatrix} u_{\mathrm{H}} \\ u_{\mathrm{T}} \end{bmatrix} \in \mathbb{R}^2. \tag{2}$$

The dynamics of the mixed-traffic vehicle platoon are governed by:

$$\dot{\mathbf{x}} = f(\mathbf{x}, v_{\mathrm{d}}) + g(\mathbf{x})\mathbf{u} + \mathbf{d}, \tag{3}$$

with $f : \mathbb{R}^n \times \mathbb{R} \to \mathbb{R}^n$, $g : \mathbb{R}^n \to \mathbb{R}^{n\times 2}$, and $\mathbf{d}(t) \in \mathbb{R}^n$ given below according to the models used for capturing the car-following motions of CAVs and HVs. We describe the longitudinal motion of HVs and two CAVs as follows.

HV dynamics: the car-following model of HV-i is given by:

$$\dot{s}_i = v_{i-1} - v_i, \tag{4}$$

$$\dot{v}_i = F_i(s_i, v_i, \dot{s}_i) + d_i. \tag{5}$$

For HV-1, since it follows the head CAV, we use the notation $v_0 = v_{\mathrm{H}}$. The acceleration function $F_i : \mathbb{R}^3 \to \mathbb{R}$ models the longitudinal driving behaviors of HV-i based on its gap s_i, speed v_i, and speed difference $\dot{s}_i$. Specifically, function F_i is a generic acceleration function that allows the adoption of many commonly-used car-following models such as the optimal velocity model (OVM) Bando et al. (1998) or the intelligent driver model (IDM) Treiber et al. (2000). In practice, human drivers often present more complex car-following behaviors that are difficult to describe accurately by simple models, and hence we use $d_i(t) \in \mathbb{R}$ to represent the unmodeled HV dynamics as an additive disturbance.

CAV dynamics: the head CAV follows an HV, and we design the driving strategy of H-CAV as a control input based on:

$$\dot{s}_{\mathrm{H}} = v_{\mathrm{d}} - v_{\mathrm{H}}, \tag{6}$$

$$\dot{v}_{\mathrm{H}} = u_{\mathrm{H}}. \tag{7}$$

In analogy, the gap s_{T} and speed v_{T} of the tail CAV are governed by:

$$\dot{s}_{\mathrm{T}} = v_N - v_{\mathrm{T}}, \tag{8}$$

$$\dot{v}_{\mathrm{T}} = u_{\mathrm{T}}, \tag{9}$$

where u_{T} controls the acceleration of the T-CAV.

For the mixed vehicle platoon controlled by the two cooperative CAVs, we thus have the system model as (3) with:

$$\begin{aligned} f(\mathbf{x}, v_{\mathrm{d}}) &= \begin{bmatrix} f_{\mathrm{H}}(\mathbf{x}, v_{\mathrm{d}}) \\ f_1(\mathbf{x}) \\ \vdots \\ f_{\mathrm{N}}(\mathbf{x}) \\ f_{\mathrm{T}}(\mathbf{x}) \end{bmatrix} \in \mathbb{R}^n, \quad f_{\mathrm{H}}(\mathbf{x}, v_{\mathrm{d}}) = \begin{bmatrix} v_{\mathrm{d}} - v_{\mathrm{H}} \\ 0 \end{bmatrix}, \quad f_i(\mathbf{x}) = \begin{bmatrix} v_{i-1} - v_i \\ F_i(s_i, v_i, v_{i-1} - v_i) \end{bmatrix}, \quad f_{\mathrm{T}}(\mathbf{x}) = \begin{bmatrix} v_N - v\mathrm{T} \\ 0 \end{bmatrix}, \\ g(\mathbf{x}) &= \begin{bmatrix} g_{\mathrm{H}} & g_{\mathrm{T}} \end{bmatrix} \in \mathbb{R}^{n\times 2}, \quad g_{\mathrm{H}} = \begin{bmatrix} 0 \\ 1 \\ 0 \\ \vdots \\ 0 \end{bmatrix} \in \mathbb{R}^n, \quad g_{\mathrm{T}} = \begin{bmatrix} 0 \\ \vdots \\ 0 \\ 0 \\ 1 \end{bmatrix} \in \mathbb{R}^n, \quad \mathbf{d} = \begin{bmatrix} 0 & 0 & 0 & d_1 & \cdots & 0 & d_N & 0 & 0 \end{bmatrix}^\top \in \mathbb{R}^n. \end{aligned} \tag{10}$$

In the following parts, we first consider the case in which the human driver's model is fully known, i.e., $d_i = 0$ in (5). In practice, if there is enough historical data and the current traffic presents a similar driving condition as historical data, we can get an accurate HV model with negligible error, which means we can take $d_i = 0$. We design controllers and analyze the stability and safety performance for $d_i = 0$. Then we analyze the robustness of the controller with an inaccurate driver's model, i.e., $d_i \neq 0$.

3. Cooperative stabilizing CAV controllers

In this section, we design stabilizing nominal controllers for the two CAVs so that stable motion of the vehicle platoon is achieved for two different notions of stability, i.e., *plant stability* and *head-to-tail string stability*.

3.1. Nonlinear cooperative control design for the head and tail CAVs

The nominal CAV controllers are designed to respond to the state $\mathbf{x}$ of the traffic and the speed v_{d} of the leader HV:

$$\begin{aligned} u_{\mathrm{H}} &= k_{\mathrm{H,n}}(\mathbf{x}, v_{\mathrm{d}}), \\ u_{\mathrm{T}} &= k_{\mathrm{T,n}}(\mathbf{x}), \end{aligned} \tag{11}$$

where subscript n stands for nominal, and the expressions of the nominal head and tail CAV controllers, $k_{\mathrm{H,n}} : \mathbb{R}^n \times \mathbb{R} \to \mathbb{R}$ and $k_{\mathrm{T,n}} : \mathbb{R}^n \to \mathbb{R}$, are chosen as follows. The controller of each CAV is designed to consist of three parts: (i) adaptive cruise control (ACC) based on the preceding vehicle; (ii) state feedback of the middle HVs that are connected to the CAV (if there are any); and (iii) cooperative response to the other CAV. If there is no connectivity between the CAV pair and HVs, the control strategy of the two CAVs will fall back to the simple ACC. We denote the set of middle HVs that are connected to the head CAV as $\mathcal{N}_{\mathrm{H}} \subseteq \{1, 2, \dots, N\}$. The controller of the H-CAV is given by:

$$k_{\mathrm{H,n}}(\mathbf{x}, v_{\mathrm{d}}) = \underbrace{\alpha_{\mathrm{H}}(V_{\mathrm{H}}(s_{\mathrm{H}}) - v_{\mathrm{H}}) + \beta_{\mathrm{H,d}}(W(v_{\mathrm{d}}) - v_{\mathrm{H}})}_{\text{Adaptive cruise control}} + \underbrace{\sum_{i \in \mathcal{N}_{\mathrm{H}}} \beta_{\mathrm{H},i}(W(v_i) - v_{\mathrm{H}})}_{\text{HV feedback}} + \underbrace{\beta_{\mathrm{H,T}}(W(v_{\mathrm{T}}) - v_{\mathrm{H}})}_{\text{CAV cooperation}}. \tag{12}$$

The first two terms are the response to the preceding vehicle, the third term is the response to the middle HVs (that is omitted if no HVs are connected to the head CAV, i.e., $\mathcal{N}_{\mathrm{H}} = \emptyset$), and the fourth term is the response to the tail CAV. We propose this controller by extending the design in Guo et al. (2023) with response to the middle HVs. Parameters $\beta_{\mathrm{H,d}}$, $\beta_{\mathrm{H},i}$, and $\beta_{\mathrm{H,T}}$ are the control gains with respect to the speeds of the head HV, middle HVs, and the tail CAV, respectively. The function $W : \mathbb{R} \to \mathbb{R}$ is defined as:

$$W(v) = \min\{v, v_{\max}\}, \tag{13}$$

with $v_{\max}$ being the maximum speed. The control gain α_{H} adjusts the head CAV's acceleration with respect to the desired speed $V_{\mathrm{H}}(s_{\mathrm{H}})$ based on the gap s_{H}. Function $V_{\mathrm{H}} : \mathbb{R} \to \mathbb{R}$ is given below.

The tail CAV's acceleration is controlled as:

$$k_{\mathrm{T,n}}(\mathbf{x}) = \underbrace{\alpha_{\mathrm{T}}(V_{\mathrm{T}}(s_{\mathrm{T}}) - v_{\mathrm{T}}) + \beta_{\mathrm{T},N}(W(v_N) - v_{\mathrm{T}})}_{\text{Adaptive cruise control}} + \underbrace{\sum_{i \in \mathcal{N}_{\mathrm{T}}} \beta_{\mathrm{T},i}(W(v_i) - v_{\mathrm{T}})}_{\text{HV feedback}} + \underbrace{\beta_{\mathrm{T,H}}(W(v_{\mathrm{H}}) - v_{\mathrm{T}})}_{\text{CAV cooperation}}, \tag{14}$$

where the meaning of each term in (14) is analogous to that in (12). In the controller (14), $\mathcal{N}_{\mathrm{T}} \subseteq \{1, 2, \dots, N-1\}$ denotes the set of middle HVs that are connected to the tail CAV excluding the preceding HV-N (and the third term is omitted if no HVs are connected to the tail CAV, i.e., $\mathcal{N}_{\mathrm{T}} = \emptyset$). Parameters α_{T}, $\beta_{\mathrm{T},N}$, $\beta_{\mathrm{T},i}$, and $\beta_{\mathrm{T,H}}$ are the corresponding control gains, while $V_{\mathrm{T}}(s_{\mathrm{T}})$ is a desired speed based on the gap s_{T}.

The gap-dependent desired speeds V_{H} and V_{T} can be designed for each CAV separately. For instance, they may be chosen differently by vehicle manufactures. The upcoming analysis is conducted for general V_{H} and V_{T} functions. For numerical examples, we will use the same range policy:

$$V_{\mathrm{H}}(s) = V_{\mathrm{T}}(s) = \begin{cases} 0, & s \le s_{\mathrm{st}}, \\ \kappa(s - s_{\mathrm{st}}), & s_{\mathrm{st}} < s < s_{\mathrm{go}}, \\ v_{\max}, & s \ge s_{\mathrm{go}}, \end{cases} \tag{15}$$

where s_{st} and s_{go} are the standstill gap and free-driving gap, respectively, and $\kappa = v_{\max}/(s_{\mathrm{go}} - s_{\mathrm{st}})$.

With the controller (11), the dynamics (3) of the mixed vehicle platoon become:

$$\dot{\mathbf{x}} = F(\mathbf{x}, v_{\mathrm{d}}) = f(\mathbf{x}, v_{\mathrm{d}}) + g_{\mathrm{H}} k_{\mathrm{H,n}}(\mathbf{x}, v_{\mathrm{d}}) + g_{\mathrm{T}} k_{\mathrm{T,n}}(\mathbf{x}), \tag{16}$$

where $F(\mathbf{x}, v_{\mathrm{d}})$ represents the car-following dynamics of the HV model and the proposed CAV controllers. Next, we analyze these dynamics, and we design the control gains denoted by α and β for the two CAVs such that their controllers achieve stable motion for the vehicle platoon. The linear stability is analyzed. We provide stability charts that identify the control gains for stability guarantees.

3.2. Stability analysis

We analyze the stability by considering the behavior of the mixed-autonomy traffic system (16) around its equilibrium. At the equilibrium, each vehicle in the vehicle platoon has the same constant speed v^* and keeps a constant gap. The equilibrium gap for each HV, s_i^*, is given by $F_i(s_i^*, v^*, 0) = 0$. For the H-CAV and T-CAV, their equilibrium gaps s_{H}^* and s_{T}^* are given by $V_{\mathrm{H}}(s_{\mathrm{H}}^*) = v^*$ and $V_{\mathrm{T}}(s_{\mathrm{T}}^*) = v^*$, respectively. For the system (16), the equilibrium state is

$$\mathbf{x}^* = [s_{\mathrm{H}}^*, v^*, s_1^*, v^*, \cdots, s_N^*, v^*, s_{\mathrm{T}}^*, v^*]^\top, \tag{17}$$

and it satisfies $F(\mathbf{x}^*, v^*) = 0$.

We analyze stability by considering that speeds and gaps fluctuate around their equilibrium values. The perturbations are described by: $\tilde{v}_{\mathrm{d}} = v_{\mathrm{d}} - v^*$, $\tilde{s}_{\mathrm{H}} = s_{\mathrm{H}} - s^*$, $\tilde{v}_{\mathrm{H}} = v_{\mathrm{H}} - v^*$, $\tilde{s}_{\mathrm{T}} = s_{\mathrm{T}} - s_{\mathrm{T}}^*$, $\tilde{v}_{\mathrm{T}} = v_{\mathrm{T}} - v^*$, $\tilde{s}_i = s_i - s_i^*$, and $\tilde{v}_i = v_i - v^*$, which are written compactly as:

$$\tilde{\mathbf{x}}(t) = \mathbf{x}(t) - \mathbf{x}^*, \quad \tilde{v}_{\mathrm{d}} = v_{\mathrm{d}} - v^*. \tag{18}$$

By linearizing the mixed traffic system (16), the evolution of these perturbations is given in the form:

$$\dot{\tilde{\mathbf{x}}} = A\tilde{\mathbf{x}} + B\tilde{v}_{\mathrm{d}}. \tag{19}$$

This linearized system, with the expressions of $A \in \mathbb{R}^{n\times n}$ and $B \in \mathbb{R}^n$, is derived in Appendix A as (A.7). We consider two types of stability for the linearized system: plant stability and head-to-tail string stability.

Definition 1 (Plant stability). System (19) is plant stable if it is asymptotically stable for $\tilde{v}_{\mathrm{d}}(t) = 0$.

Definition 2 (Head-to-tail string stability). System (19) is head-to-tail string stable if $\sqrt{\int_0^\infty \tilde{v}_{\mathrm{T}}(t)^2\,\mathrm{d}t} < \sqrt{\int_0^\infty \tilde{v}_{\mathrm{d}}(t)^2\,\mathrm{d}t}$ for any square integrable $\tilde{v}_{\mathrm{d}}$ and $\tilde{\mathbf{x}}(0) = 0$.

Remark 1 (Plant and string stability). Plant stability refers to the *internal* dynamics of the system when the external disturbance is $\tilde{v}_{\mathrm{d}} = 0$, while head-to-tail string stability describes the system's response to the *external* disturbance $\tilde{v}_{\mathrm{d}}$ when the initial state is $\tilde{\mathbf{x}}(0) = 0$. With respect to their implications for the mixed traffic system, plant stability means that, when the downstream traffic travels at the equilibrium speed v^*, the platoon will approach the equilibrium state $\mathbf{x}^*$ associated with the same speed v^* and constant spacing for each vehicle. Head-to-tail string stability, on the other hand, requires that when the leader HV has some speed perturbation $\tilde{v}_{\mathrm{d}}$ the tail CAV will experience a smaller perturbation $\tilde{v}_{\mathrm{T}}$ in its speed, i.e., the speed perturbations in downstream traffic are attenuated by the vehicle platoon and the traffic becomes smoother. For traffic systems, head-to-tail string stability is a more restrictive performance requirement than plant stability.

We analyze plant and head-to-tail string stability using the *head-to-tail transfer function* defined as:

$$G(s) = \frac{\widetilde{V}_{\mathrm{T}}(s)}{\widetilde{V}_{\mathrm{d}}(s)}, \tag{20}$$

with $\widetilde{V}_{\mathrm{T}}(s)$ and $\widetilde{V}_{\mathrm{d}}(s)$ being the Laplace transforms of the speed perturbations of the leader HV, $\tilde{v}_{\mathrm{d}}$, and the tail CAV, $\tilde{v}_{\mathrm{T}}$, respectively. The head-to-tail transfer function $G(s)$ of the linearized system (19) is derived in Appendix A. Its final expression is:

$$G(s) = \frac{N(s)}{D(s)}, \tag{21}$$

where the numerator is given by:

$$N(s) = (\beta_{\mathrm{H,d}}s + \xi_{\mathrm{H}})\left(\beta_{\mathrm{T,H}}sP_0 + (\beta_{\mathrm{T,N}}s + \xi_{\mathrm{T}})P_{\mathrm{N}} + \sum_{i\in\mathcal{N}_{\mathrm{T}}} \beta_{\mathrm{T},i}sP_i\right), \tag{22}$$

with $\xi_{\mathrm{H}} = \alpha_{\mathrm{H}}V_{\mathrm{H}}'(s_{\mathrm{H}}^*)$, $\xi_{\mathrm{T}} = \alpha_{\mathrm{T}}V_{\mathrm{T}}'(s_{\mathrm{T}}^*)$, while the denominator is:

$$D(s) = \left((s^2 + \eta_{\mathrm{H}}s + \xi_{\mathrm{H}})P_0 - \sum_{i\in\mathcal{N}_{\mathrm{H}}} \beta_{\mathrm{H},i}sP_i\right)(s^2 + \eta_{\mathrm{T}}s + \xi_{\mathrm{T}}) - \beta_{\mathrm{H,T}}s\left(\beta_{\mathrm{T,H}}sP_0 + (\beta_{\mathrm{T,N}}s + \xi_{\mathrm{T}})P_{\mathrm{N}} + \sum_{i\in\mathcal{N}_{\mathrm{T}}} \beta_{\mathrm{T},i}sP_i\right), \tag{23}$$

with $\eta_{\mathrm{H}} = \alpha_{\mathrm{H}} + \beta_{\mathrm{H,d}} + \sum_{i\in\mathcal{N}_{\mathrm{H}}} \beta_{\mathrm{H},i} + \beta_{\mathrm{H,T}}$, $\eta_{\mathrm{T}} = \alpha_{\mathrm{T}} + \beta_{\mathrm{T,N}} + \sum_{i\in\mathcal{N}_{\mathrm{T}}} \beta_{\mathrm{T},i} + \beta_{\mathrm{T,H}}$, and:

$$P_0 = \prod_{j=1}^{N}(s^2 + a_{j2}s + a_{j1}), \quad P_i = \prod_{j=1}^{i}(a_{j3}s + a_{j1}) \prod_{j=i+1}^{N}(s^2 + a_{j2}s + a_{j1}), \quad P_N = \prod_{j=1}^{N}(a_{j3}s + a_{j1}), \tag{24}$$

where $a_{j1} = \frac{\partial F_j}{\partial s_j}(s_j^*, v^*, 0)$, $a_{j2} = \frac{\partial F_j}{\partial \dot{s}_j}(s_j^*, v^*, 0) - \frac{\partial F_j}{\partial v_j}(s_j^*, v^*, 0)$, $a_{j3} = \frac{\partial F_j}{\partial \dot{s}_j}(s_j^*, v^*, 0)$.

Note that the expressions in (24) represent the dynamics (4)-(5) of HVs. Meanwhile, the formulas in (22) and (23) are determined by the CAV controllers in (12) and (14), and hence they depend on the α and β controller gains. Using the head-to-tail transfer function $G(s)$, we provide the conditions on these controller gains to stabilize the linearized system (19). This implies local stability for the nonlinear system (16), i.e., when the system state and disturbance are within a small region around the equilibrium. The stability conditions are summarized in Theorem 1.

Theorem 1. *System (19) is plant stable if the controller gains α_{H}, $\beta_{\mathrm{H,d}}$, $\beta_{\mathrm{H},i}$, $\beta_{\mathrm{H,T}}$, α_{T}, $\beta_{\mathrm{T,N}}$, $\beta_{\mathrm{T},i}$, $\beta_{\mathrm{T,H}}$ are chosen such that all solutions of $D(s) = 0$ have negative real parts, where D is given in (23). The system is head-to-tail string stable if $|G(\mathrm{j}\omega)| < 1$ holds for all $\omega > 0$, where $\mathrm{j}^2 = -1$ and G is given in (21)-(23).*

3.3. Stabilizing control gains

Here we use Theorem 1 to determine the range of controller gains that stabilize the system, and we plot this range as *stability charts* in the $(\beta_{\mathrm{H,T}}, \beta_{\mathrm{T,H}})$ plane of controller gains. The corresponding stability boundaries (which bound the region of stabilizing controller gains) are given as follows.

The mixed traffic system is at the plant-stability boundary when $D(s) = 0$ has a real root at the origin, i.e., $s = 0$, or has a complex conjugate pair of roots $s = \pm\mathrm{j}\omega$ with $\omega > 0$. For these two cases, the stability boundaries are given in Corollary 1.

Corollary 1 (Plant stability boundary). *The plant stability boundaries of system (19) are given by:*

$$D(0) = 0. \tag{25}$$

and:

$$\begin{aligned} \mathrm{Re}(D(\mathrm{j}\omega)) &= 0, \\ \mathrm{Im}(D(\mathrm{j}\omega)) &= 0, \end{aligned} \tag{26}$$

with $\mathrm{Re}(\cdot)$ *and* $\mathrm{Im}(\cdot)$ *being the real and imaginary parts of a complex number, and* D *is given in (23).*

Based on Theorem 1, the head-to-tail string stability condition is $|G(\mathrm{j}\omega)| < 1$ for all $\omega > 0$. We note that $|G(0)| = 1$. Therefore, there are two cases for the string stability boundaries Guo et al. (2023). In the first case, $|G(\mathrm{j}\omega)|$ gets its maximum value at $\omega = 0$. In the second case, $|G(\mathrm{j}\omega)| = 1$ for some positive $\omega > 0$. We provide the string stability boundaries for these two cases in Corollary 2.

Corollary 2 (Head-to-tail string stability boundary). *The head-to-tail string stability boundaries of system (19) are given by:*

$$\lim_{\omega \to 0^+} \frac{1}{\omega^2} \left(|D(\mathrm{j}\omega)|^2 - |N(\mathrm{j}\omega)|^2 \right) = 0, \tag{27}$$

and by a family of curves parameterized by the wave number $\theta \in [0, 2\pi)$*, obtained from:*

$$G(\mathrm{j}\omega) = e^{-\mathrm{j}\theta}, \tag{28}$$

which is equivalent to:

$$\begin{aligned} &\mathrm{Re}(D(\mathrm{j}\omega)) - \mathrm{Re}(N(\mathrm{j}\omega)) \cos\theta + \mathrm{Im}(N(\mathrm{j}\omega)) \sin\theta = 0, \\ &\mathrm{Im}(D(\mathrm{j}\omega)) - \mathrm{Re}(N(\mathrm{j}\omega)) \sin\theta - \mathrm{Im}(N(\mathrm{j}\omega)) \cos\theta = 0. \end{aligned} \tag{29}$$

Here G*,* N*, and* D *are given in (21)–(23).*

Equations (25)–(26) and (27)–(29) define the plant and string stability boundaries, respectively. Note that the left-hand sides of these equations depend on the control gains like $\beta_{\mathrm{H,T}}$ and $\beta_{\mathrm{T,H}}$. Thus, these equations define curves in the space of controller gains such as in the $(\beta_{\mathrm{H,T}}, \beta_{\mathrm{T,H}})$ plane. By plotting these curves, we create stability charts that identify stabilizing gains.

As a numerical example, we consider a vehicle platoon of $N = 4$ middle HVs. For the CAV spacing policy in (15), we use $s_{\mathrm{st}} = 2$ m, $s_{\mathrm{go}} = 40$ m, and $v_{\max} = 40$ m/s. We set the HV dynamics as the optimal velocity model:

$$F_i(s_i, v_i, \dot{s}_i) = a(V_i(s_i) - v_i) + b\dot{s}_i, \tag{30}$$

where $a > 0$ and $b > 0$ reflect the human driver's reaction to match its speed v_i to the desired speed $V_i(s_i)$ and the preceding vehicle's speed v_{i-1}, respectively. For the human drivers, we take the desired speed $V_i(s)$ also in the form of (15), but with s_{st} and s_{go} calibrated from trajectories in the NGSIM dataset Fhwa (2007). We calibrate the model parameters for HVs as $a = 0.16\ \mathrm{s}^{-1}$, $b = 0.61\ \mathrm{s}^{-1}$, $s_{\mathrm{st}} = 1.9$ m, and $s_{\mathrm{go}} = 46.3$ m. We set the equilibrium speed of the vehicle platoon as $v^* = 20$ m/s, which gives the equilibrium gap for the HVs as $s_i^* = 24$ m and for the two CAVs as $s_{\mathrm{H}}^* = s_{\mathrm{T}}^* = 21$ m.

Fig. 2 presents *stability charts* that indicate the stability boundaries and the range of cooperative CAV controller gains in the $(\beta_{\mathrm{H,T}}, \beta_{\mathrm{T,H}})$ domain that lead to plant and head-to-tail string stability.

Remark 2 (Stability impact of ACC mode only). Fig. 2(a) considers the case where the middle HVs are not connected. In this case, if the two CAVs are also not connected (i.e., $\beta_{\mathrm{H,T}} = 0$, $\beta_{\mathrm{T,H}} = 0$), then the two CAVs execute ACC, and the vehicle platoon is string unstable. This means that when the head HV has some speed perturbations, the tail CAV will experience a larger speed perturbation through propagation along the vehicle platoon.

Remark 3 (Stability impact of CAV cooperation).

In Fig. 2(a), by connecting the two CAVs and using feedback gains $(\beta_{\mathrm{H,T}}, \beta_{\mathrm{T,H}})$ within the string stable region shaded in red, the mixed vehicle platoon becomes head-to-tail string stable. This is possible only if the tail CAV's controller responds to the head CAV (i.e., string stability requires $\beta_{\mathrm{T,H}} \neq 0$), while the response of the head CAV to the tail CAV is not necessary (i.e., there exist string stable gains even when $\beta_{\mathrm{H,T}} = 0$). As Fig. 2(a) shows, by choosing proper CAV cooperation feedback gains $(\beta_{\mathrm{H,T}}, \beta_{\mathrm{T,H}})$, the system is already head-to-tail string stable without HV connection. This highlights that the proposed controller stabilizes traffic even in the most challenging case where all HVs are not equipped with communication devices.

If HVs are connected and middle HV feedback is included, the stability region is further enlarged as in Fig. 2(b). In this case, smaller controller gains can be chosen, which may reduce accelerations and increase passenger comfort. Furthermore, if the tail CAV includes feedback from middle HVs, as in Fig. 2(b), then the system can be rendered string stable even if the two CAVs are not connected (i.e., $\beta_{\mathrm{H,T}} = 0$ and $\beta_{\mathrm{T,H}} = 0$). This shows that for string stability, the tail CAV should include feedback from its downstream traffic, either from the head CAV or the middle HVs. Fig. 2(c) shows how the stability region is affected when the head CAV includes middle HV feedback in its controller. Similar to Fig. 2(a), the system can be string stable even with $\beta_{\mathrm{H,T}} = 0$ if $\beta_{\mathrm{T,H}}$ is properly chosen, i.e., the head CAV can ignore tail CAV's feedback but not vice versa.

Remark 4 (Stability impact of connecting HVs). Fig. 2(d) compares the string stability boundaries from Fig. 2(a)-(c) that correspond to different communication topologies of HV connection. Yellow color indicates when the CAVs are not connected to HVs (cf. panel (a)), red shows when the tail CAV looks ahead and connects to HVs (cf. panel (b)), and green corresponds to when the head CAV

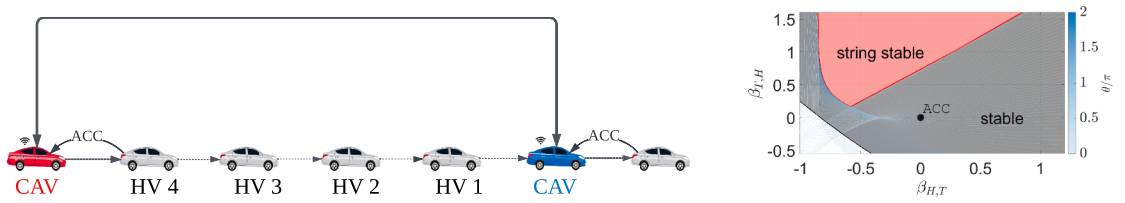

(a) No HV connection

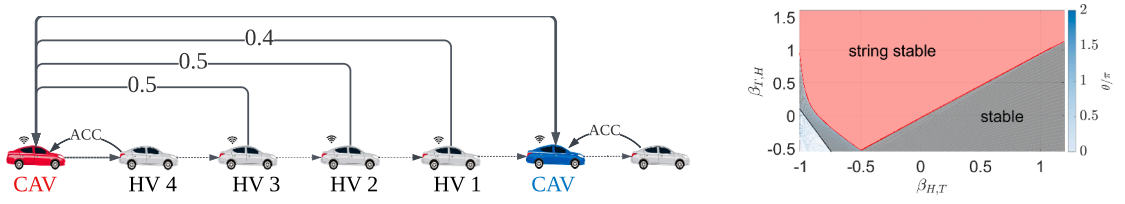

(b) Tail CAV looks ahead, i.e., HVs are connected to T-CAV

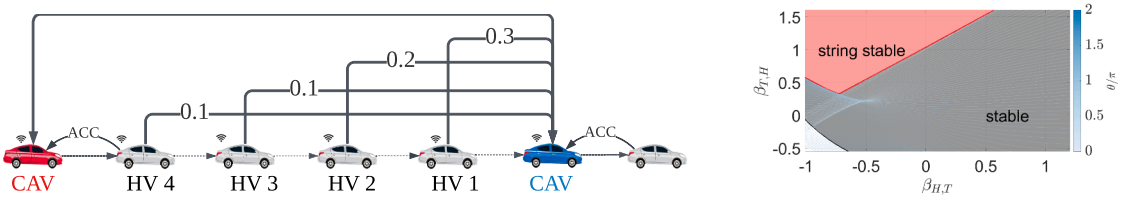

(c) Head CAV looks behind, i.e., HVs are connected to H-CAV

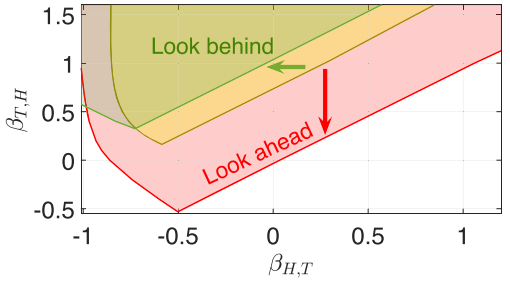

Fig. 2. Stability charts in the $(\beta_{H,T}, \beta_{T,H})$ space of control gains. Grey areas and red areas represent plant stability and head-to-tail string stability, respectively. The white area represents the unstable region. In panel (a), the middle HVs are not connected and the CAVs do not respond to them. In panel (b), HV 1, HV 2, and HV 3 are connected to the tail CAV who responds to them with gains $\beta_{T,1} = 0.4$, $\beta_{T,2} = 0.5$, $\beta_{T,3} = 0.5$ (while also responding to HV-4 based on range sensors). In panel (c), HVs are connected to the head CAV who responds to them with controller gains $\beta_{H,1} = 0.3$, $\beta_{H,2} = 0.2$, $\beta_{H,3} = 0.1$, $\beta_{H,4} = 0.1$. In all the three cases, the remaining controller gains are $\alpha_H = 0.4$, $\beta_{H,d} = 0.6$, $\alpha_T = 0.4$, and $\beta_{T,4} = 0.6$. In panel (d), the stability charts from panels (a)-(c) are compared. (For interpretation of the references to colour in this figure legend, the reader is referred to the web version of this article.)

looks behind and connects to HVs (cf. panel (c)). By connecting HVs to CAVs, the string stability boundaries drift as the arrows show. In this numerical example, "look ahead" makes stabilization easier when cooperating the two CAVs while "look behind" does not necessarily imply that. For various communication topologies, there exists a large overlap of the string stability regions, from which we can select the controller gains $\beta_{H,T}$ and $\beta_{T,H}$ to stabilize traffic.

4. Safety-critical control

In this section, we first define the safety impact of the proposed cooperative CAV controllers (12) and (14), and then analyze how the choice of controller gains affects safety. Secondly, we utilize control barrier functions to design safety filters that constrain control inputs in real-time for safety guarantees. This is realized by formulating and solving an optimization problem that modifies the operation of potentially unsafe nominal controller designs.

4.1. Longitudinal safety of CAVs and HVs

In longitudinal car-following control, safety refers to eliminating the risk of rear-end collision. We adopt surrogate safety measures Wang et al. (2021) to evaluate the risk of collision for CAVs and HVs in various traffic scenarios. To this end, we adopt the

constant time headway (CTH) safe spacing policy Zhao et al. (2023) for the safety definition of the CAVs and middle HVs. For a vehicle with speed v and gap s, the CTH policy requires that the gap exceeds a minimum safe value which is the product of a safe time headway $\tau > 0$ and the speed:

$$s \geq \tau v. \tag{31}$$

For the head CAV, we set its safe time headway as $\tau_{\mathrm{H}} > 0$, and the CTH policy constrains its spacing s_{H} and speed v_{H} as:

$$s_{\mathrm{H}} \geq \tau_{\mathrm{H}} v_{\mathrm{H}}. \tag{32}$$

This yields a safe set, i.e., a set of states where the head CAV is considered to be safe:

$$C_{\mathrm{H}} = \{\mathbf{x} \in \mathbb{R}^n : h_{\mathrm{H}}(\mathbf{x}) \geq 0\}, \tag{33}$$

with the safety function h_{H} being:

$$h_{\mathrm{H}}(\mathbf{x}) = s_{\mathrm{H}} - \tau_{\mathrm{H}} v_{\mathrm{H}}. \tag{34}$$

To guarantee safety, the controller should be designed so that if the head CAV is safe initially then it stays safe for all future time. That is, if $\mathbf{x}(0) \in C_{\mathrm{H}}$, then $\mathbf{x}(t) \in C_{\mathrm{H}}$ holds for all $t \geq 0$, which means that the safe set C_{H} is *forward invariant*. For the tail CAV, similarly, we take a safe time headway as $\tau_{\mathrm{T}} > 0$, and define its safe set as:

$$C_{\mathrm{T}} = \{\mathbf{x} \in \mathbb{R}^n : h_{\mathrm{T}}(\mathbf{x}) \geq 0\}, \tag{35}$$

with the safety function:

$$h_{\mathrm{T}}(\mathbf{x}) = s_{\mathrm{T}} - \tau_{\mathrm{T}} v_{\mathrm{T}}. \tag{36}$$

We aim to ensure forward invariance of C_{T}, i.e., if $\mathbf{x}(0) \in C_{\mathrm{T}}$, then $\mathbf{x}(t) \in C_{\mathrm{T}}$ for all $t \geq 0$. For HV i, we take its safe time headway as τ_i, and the CTH spacing policy yields the safety function:

$$h_i(\mathbf{x}) = s_i - \tau_i v_i. \tag{37}$$

Remark 5 (Safety evaluation). The safety function h acts as a safety surrogate measurement, and a negative h implies an unsafe car-following scenario that has a higher risk of collision. When $h < 0$, the gap s may still be positive. A negative gap s means that a severe collision has happened. In the following analysis, we refer to the CAVs or HVs as "safe" if $h \geq 0$.

4.2. Safety impact of the nominal controller

The forward invariance of the safe sets C_{H} and C_{T} for the mixed traffic system (3) is established using Nagumo's theorem.

Lemma 1 (Nagumo's theorem Nagumo (1942)). *Consider the system:*

$$\dot{\mathbf{x}} = F(\mathbf{x}), \tag{38}$$

with state $\mathbf{x} \in \mathbb{R}^n$, safe set C, and safety function $h : \mathbb{R}^n \to \mathbb{R}$ such that $\nabla h(\mathbf{x}) \neq 0$ if $h(\mathbf{x}) = 0$. The system is safe w.r.t. C (that is, C is forward invariant) if and only if:

$$\dot{h}(\mathbf{x}) = \nabla h(\mathbf{x}) \cdot F(\mathbf{x}) \geq 0 \tag{39}$$

holds for all $\mathbf{x} \in \mathbb{R}^n$ satisfying $h(\mathbf{x}) = 0$.

Using condition (39) in Lemma 1, we determine the gains of the nominal controller (12) that ensure safety for the head CAV. This is summarized in Theorem 2, whose proof is given in Appendix B.

Theorem 2 (Safety of the nominal head CAV controller). *System (16) with the nominal controller (12) of the head CAV and the range policy (15) is safe w.r.t. C_{H} defined in (33)–(34), if $v_{\mathrm{d}}, v_{\mathrm{H}}, v_i, v_{\mathrm{T}} \in [0, v_{\max}]$, $s_{\mathrm{H}} \in [s_{\mathrm{st}}, s_{\mathrm{go}}]$, and if the controller parameters satisfy $\kappa \leq 1/\tau_{\mathrm{H}}$ and:*

$$\alpha_{\mathrm{H}} \geq \left(|1 - \tau_{\mathrm{H}} \beta_{\mathrm{H,d}}| + \tau_{\mathrm{H}} \sum_{i \in \mathcal{N}_{\mathrm{H}}} |\beta_{\mathrm{H},i}| + \tau_{\mathrm{H}} |\beta_{\mathrm{H,T}}| \right) \frac{v_{\max}}{s_{\mathrm{st}}}. \tag{40}$$

Remark 6 (Safe controller gains). The safety criterion (40) in Theorem 2 can be interpreted as follows. It provides safe choices of controller gains α_{H} and $\beta_{\mathrm{H,d}}$ that are related to the adaptive cruise control term in (12):

$$\frac{s_{\mathrm{st}}}{v_{\max}} \alpha_{\mathrm{H}} - |1 - \tau_{\mathrm{H}} \beta_{\mathrm{H,d}}| \geq \tau_{\mathrm{H}} \sum_{i \in \mathcal{N}_{\mathrm{H}}} |\beta_{\mathrm{H},i}| + \tau_{\mathrm{H}} |\beta_{\mathrm{H,T}}|. \tag{41}$$

It also gives a maximum safe CAV coordination gain $\beta_{\mathrm{H,T}}$ as:

$$|\beta_{\mathrm{H,T}}| \leq \frac{s_{\mathrm{st}}}{v_{\max} \tau_{\mathrm{H}}} \alpha_{\mathrm{H}} - \left| \frac{1}{\tau_{\mathrm{H}}} - \beta_{\mathrm{H,d}} \right| - \sum_{i \in \mathcal{N}_{\mathrm{H}}} |\beta_{\mathrm{H},i}|. \tag{42}$$

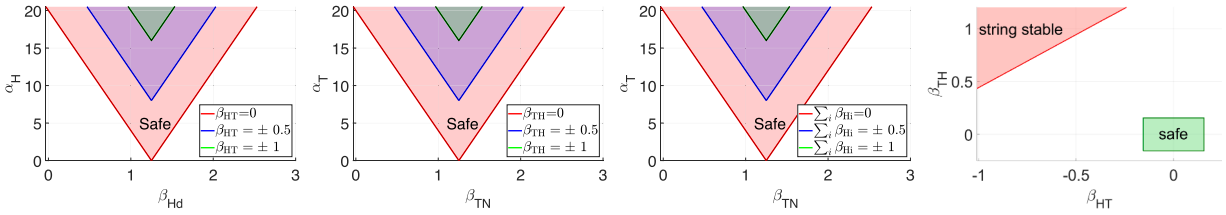

(a) Safe gains for head CAV (b) Safe gains for tail CAV (c) Safe gains for tail CAV (d) Safe and stable gains for CAV cooperation

Fig. 3. Safety charts in the space of control gains for the nominal controller (12)–(14). (a) Safe $(\beta_{\mathrm{H,d}}, \alpha_{\mathrm{H}})$ gains considering the head CAV's safety (with $\beta_{\mathrm{T,H}} = 0$, $\beta_{\mathrm{H},i} = 0$, $\beta_{\mathrm{T},i} = 0$, and safe time headway $\tau_{\mathrm{H}} = 0.8$ s); (b) safe $(\beta_{\mathrm{T},N}, \alpha_{\mathrm{T}})$ gains associated with the tail CAV's safety (with $\beta_{\mathrm{H,T}} = 0$, $\beta_{\mathrm{H},i} = 0$, $\beta_{\mathrm{T},i} = 0$, and safe time headway $\tau_{\mathrm{T}} = 0.8$ s); (c) safe $(\beta_{\mathrm{T},N}, \alpha_{\mathrm{T}})$ gains for different $\beta_{\mathrm{H},i}$ HV feedback gains (with $\beta_{\mathrm{H,T}} = 0$, $\beta_{\mathrm{T,H}} = 0$, $\beta_{\mathrm{T},i} = 0$); and (d) safe $(\beta_{\mathrm{H,T}}, \beta_{\mathrm{T,H}})$ gains for the safety of both CAVs (with $\beta_{\mathrm{H},i} = 0$, $\beta_{\mathrm{T},i} = 0$). The spacing policy $V(s)$ is the same as in Fig. 2. The shaded region indicates the range of gains that ensure safety for the respective CAVs based on Theorems 2 and 3. Notice that the gains of the nominal controller are restricted if one intends to achieve provably safe behavior (i.e., α_{H} and α_{T} must be very high or $\beta_{\mathrm{H,T}}$ and $\beta_{\mathrm{T,H}}$ must be very small). This motivates the introduction of safety filters to enforce safe behaviors by deviating from the nominal controller to prevent safety violation.

Such a $\beta_{\mathrm{H,T}}$ gain exists only if the right-hand side is non-negative. When $\beta_{\mathrm{H},i} = 0$ and $\beta_{\mathrm{H,d}} = 1/\tau_{\mathrm{H}}$, the right-hand side has the maximum as $\alpha_{\mathrm{H}} s_{\mathrm{st}}/(v_{\max}\tau_{\mathrm{H}})$. Similarly, condition (40) also provides safe gains considering the feedback of HV states:

$$\sum_{i\in\mathcal{N}_{\mathrm{H}}} |\beta_{\mathrm{H},i}| \le \frac{s_{\mathrm{st}}}{v_{\max}\tau_{\mathrm{H}}}\alpha_{\mathrm{H}} - \left|\frac{1}{\tau_{\mathrm{H}}} - \beta_{\mathrm{H,d}}\right| - |\beta_{\mathrm{H,T}}|, \tag{43}$$

where the right-hand side should again be non-negative to ensure the existence of such $\beta_{\mathrm{H},i}$. When $\beta_{\mathrm{H,d}} = 1/\tau_{\mathrm{H}}$ and $\beta_{\mathrm{H,T}} = 0$, the right-hand side has the maximum as $\alpha_{\mathrm{H}} s_{\mathrm{st}}/(v_{\max}\tau_{\mathrm{H}})$.

To ensure safety for the tail CAV, the nominal controller (14) must satisfy similar criteria given in Theorem 3. The proof of this theorem follows the same steps as for Theorem 2, hence it is omitted.

Theorem 3 (Safety of the nominal tail CAV controller). *System (3) with the nominal controller (14) of the tail CAV and the range policy (15) is safe w.r.t. C_{T} defined in (35)–(36), if $v_{\mathrm{d}}, v_{\mathrm{H}}, v_i, v_{\mathrm{T}} \in [0, v_{\max}]$, $s_{\mathrm{T}} \in [s_{\mathrm{st}}, s_{\mathrm{go}}]$, and if the controller parameters satisfy $\kappa \le 1/\tau_{\mathrm{T}}$ and:*

$$\alpha_{\mathrm{T}} \ge \left(|1 - \tau_{\mathrm{T}}\beta_{\mathrm{T,N}}| + \tau_{\mathrm{T}} \sum_{i\in\mathcal{N}_{\mathrm{T}}} |\beta_{\mathrm{T},i}| + \tau_{\mathrm{T}}|\beta_{\mathrm{T,H}}|\right)\frac{v_{\max}}{s_{\mathrm{st}}}. \tag{44}$$

The range of safe controller gains provided by Theorems 2 and 3 is depicted as *safety charts* in Fig. 3.

Remark 7 (Safety impact of CAV cooperation)**.**
The shaded domain in Fig. 3(a) shows the safe controller gains for the head CAV in the $(\beta_{\mathrm{H,d}}, \alpha_{\mathrm{H}})$ space for various values of $\beta_{\mathrm{H,T}}$ based on (40). It can be observed that including the cooperation with the tail CAV (i.e., taking $\beta_{\mathrm{H,T}} \neq 0$) makes the safety region shift towards higher α_{H} gains. Similarly, Fig. 3(b) shows the safe gains for the tail CAV in the $(\beta_{\mathrm{T},N}, \alpha_{\mathrm{T}})$ space for various $\beta_{\mathrm{T,H}}$ values based on (44). The same trend is showcased: the safety region shifts up by including the cooperation with the head CAV ($\beta_{\mathrm{T,H}} \neq 0$).

Remark 8 (Safety impact of connecting HVs)**.** We plot the safe ACC gains for the head CAV in Fig. 3(c). When the CAV includes feedback from middle HVs, its safety region shifts up and requires larger α_{H}. The effect of HV feedback on the tail CAV safety is also similar, and we omit the corresponding figure.

Remark 9 (Trade-off between stability and safety)**.**
The cooperation between CAVs enhances stability as in Remark 3 but makes it harder to guarantee safety as in Remark 7. This trade-off also exists in the connectivity of HVs. Based on Remark 4 and Fig. 2, the stability region grows by setting proper controller gains for the feedback of HV states. Meanwhile, Remark 8 shows that the selection of safe gains becomes more limited by connecting to HVs (i.e., the right-hand sides of (40) and (44) increase for $\beta_{\mathrm{H},i} \neq 0$ and $\beta_{\mathrm{T},i} \neq 0$).

Fig. 3(d) indicates the safe CAV cooperation gains in green in the $(\beta_{\mathrm{H,T}}, \beta_{\mathrm{T,H}})$ space considering the safety of both CAVs. We set $\alpha_{\mathrm{H}} = 1$, $\alpha_{\mathrm{T}} = 1$. We consider no HV connection, i.e., $\beta_{\mathrm{H},i} = 0$, $\beta_{\mathrm{T},i} = 0$, and we set $\beta_{\mathrm{H,d}} = 1/\tau_{\mathrm{H}}$, $\beta_{\mathrm{T,N}} = 1/\tau_{\mathrm{T}}$, which gives the maximum range of safe CAV coordination gains $\beta_{\mathrm{H,T}}$ and $\beta_{\mathrm{T,H}}$; see Remark 6. We also plot the string-stability region as the red region. As Fig. 3(d) shows, the string stability region and safety region do not intersect. This highlights that guaranteeing both stability and safety by the nominal controller (12)–(14) may not be possible. Furthermore, Fig. 3(a,b,c) also demonstrate that cooperating CAVs require a very high α gain for provable safety (for example, the blue curve in panel (a) shows that the head CAV is safe only for $\alpha_{\mathrm{H}} > 5$ when the CAV cooperation gain is set to $\beta_{\mathrm{H,T}} = 0.5$). Such high α gain is undesired and infeasible for practical CAV control applications. Experiments in Alan et al. (2024) have shown that the gap-related controller gain α is recommended to be smaller than 1. Therefore, these restrictions on the safe control gains motivate the modification of the nominal controller (12)–(14) to actively enforce safety. This is discussed in the next subsections through the introduction of CBF-based safety filters.

4.3. Preliminaries on CBFs

Control barrier functions provide a general tool to constrain the control input to ensure safety. We present the basics of CBFs as follows. Consider an affine control system with state $\mathbf{x} \in \mathbb{R}^n$ and control input $\mathbf{u} \in \mathbb{R}^m$:

$$\dot{\mathbf{x}} = f(\mathbf{x}) + g(\mathbf{x})\mathbf{u}, \tag{45}$$

cf. (3), with controller $\mathbf{u} = k(\mathbf{x})$ and initial condition $\mathbf{x}(0) = \mathbf{x}_0 \in \mathbb{R}^n$. If f, g, and k are locally Lipschitz, the system has a unique solution $\mathbf{x}(t)$, which we assume to exist for all $t \geq 0$. The system is safe if the solution stays in a safe set $\mathcal{C}$, i.e., $\mathbf{x}(t) \in \mathcal{C}$ holds for all $t \geq 0$ if $\mathbf{x}_0 \in \mathcal{C}$. Let $\mathcal{C}$ be given by a continuously differentiable function $h : \mathbb{R}^n \to \mathbb{R}$, cf. (33) and (35).

Definition 3 (Control Barrier Function Ames et al. (2019)). Function h is called a control barrier function for the system (45) on $\mathcal{C}$ if there exists an extended class-$\mathcal{K}_\infty$ function γ such that:

$$\sup_{\mathbf{u}\in\mathbb{R}^m} L_f h(\mathbf{x}) + L_g h(\mathbf{x})\mathbf{u} > -\gamma(h(\mathbf{x})), \quad \forall \mathbf{x} \in \mathcal{C}, \tag{46}$$

with $L_f h(\mathbf{x}) = \nabla h(\mathbf{x}) \cdot f(\mathbf{x})$ and $L_g h(\mathbf{x}) = \nabla h(\mathbf{x}) \cdot g(\mathbf{x})$.

The CBF is used to guarantee safety of the closed-loop system with a feedback controller $k : \mathbb{R}^n \to \mathbb{R}^m$, $\mathbf{u} = k(\mathbf{x})$ for (45).

Theorem 4 (Safety guarantee by CBF Ames et al. (2019)). *If function h is a control barrier function for (45) on $\mathcal{C}$, then any locally Lipschitz continuous controller $\mathbf{u} = k(\mathbf{x})$ satisfying:*

$$L_f h(\mathbf{x}) + L_g h(\mathbf{x}) k(\mathbf{x}) \geq -\gamma(h(\mathbf{x})), \quad \forall \mathbf{x} \in \mathcal{C}, \tag{47}$$

renders the set $\mathcal{C}$ forward invariant (safe), i.e, $\mathbf{x}(t) \in \mathcal{C}$, $\forall t \geq 0$ holds for the closed-loop system for all $\mathbf{x}_0 \in \mathcal{C}$.

To control a system with formal safety guarantees, CBFs can be integrated with a pre-designed nominal controller such as (12) or (14). In particular, a nominal controller $\mathbf{u} = k_{\mathrm{n}}(\mathbf{x})$ can be modified in a minimal way to synthesize a safety-critical control input $\mathbf{u} = k(\mathbf{x})$, by solving the quadratic program (QP):

$$\begin{aligned} k(\mathbf{x}) = \underset{\mathbf{u}\in\mathbb{R}^m}{\operatorname{argmin}} \ & \|\mathbf{u} - k_{\mathrm{n}}(\mathbf{x})\|^2, \\ \text{s.t. } & L_f h(\mathbf{x}) + L_g h(\mathbf{x})\mathbf{u} + \gamma(h(\mathbf{x})) \geq 0, \end{aligned} \tag{48}$$

that is also called a *safety filter*. When the control input is a scalar (i.e., $\mathbf{u} \in \mathbb{R}$) and $L_g h(\mathbf{x}) < 0$ for all $\mathbf{x} \in \mathbb{R}^n$, this safety filter simplifies to the form:

$$k(\mathbf{x}) = \min\left\{ k_{\mathrm{n}}(\mathbf{x}), -\frac{L_f h(\mathbf{x}) + \gamma(h(\mathbf{x}))}{L_g h(\mathbf{x})} \right\}. \tag{49}$$

4.4. Safety filter design for CAV, HV and platoon

While Theorems 2 and 3 provide conditions on the nominal CAV controllers (12) and (14) to ensure safety, we utilize CBFs to minimally modify these nominal controllers and obtain safety-critical controllers:

$$\begin{aligned} u_{\mathrm{H}} &= k_{\mathrm{H}}(\mathbf{x}, v_{\mathrm{d}}), \\ u_{\mathrm{T}} &= k_{\mathrm{T}}(\mathbf{x}), \end{aligned} \tag{50}$$

based on real-time traffic states. We consider three types of safety: CAV safety, HV safety, and platoon safety.

CAV safety: CAV safety refers to the requirement that the two CAVs keep a safe gap behind their preceding vehicles by enforcing the CTH policy. For the head CAV, the CBF h_{H} in (34) gives constraints on the controller u_{H} as:

$$L_f h_{\mathrm{H}}(\mathbf{x}, v_{\mathrm{d}}) + L_{g_{\mathrm{H}}} h_{\mathrm{H}}(\mathbf{x}) u_{\mathrm{H}} \geq -\gamma_{\mathrm{H}} h_{\mathrm{H}}(\mathbf{x}), \tag{51}$$

cf. (47), with $L_f h_{\mathrm{H}}(\mathbf{x}, v_{\mathrm{d}}) = v_{\mathrm{d}} - v_{\mathrm{H}}$, $L_{g_{\mathrm{H}}} h_{\mathrm{H}}(\mathbf{x}) = -\tau_{\mathrm{H}}$, and $\gamma_{\mathrm{H}} > 0$. This is equivalent to:

$$u_{\mathrm{H}} \leq \frac{1}{\tau_{\mathrm{H}}}(v_{\mathrm{d}} - v_{\mathrm{H}}) + \gamma_{\mathrm{H}}\left(\frac{1}{\tau_{\mathrm{H}}} s_{\mathrm{H}} - v_{\mathrm{H}}\right). \tag{52}$$

The right-hand side resembles the adaptive cruise control terms in the nominal controller (12). Based on (49), the safety filter enforcing the head CAV's safety is:

$$k_{\mathrm{H}}(\mathbf{x}, v_{\mathrm{d}}) = \min\left\{ k_{\mathrm{H,n}}(\mathbf{x}, v_{\mathrm{d}}), \frac{1}{\tau_{\mathrm{H}}}(v_{\mathrm{d}} - v_{\mathrm{H}}) + \gamma_{\mathrm{H}}\left(\frac{1}{\tau_{\mathrm{H}}} s_{\mathrm{H}} - v_{\mathrm{H}}\right) \right\}, \tag{53}$$

where the nominal controller $k_{\mathrm{H,n}}$ is given in (12). Similarly, the safety function h_{T} of the tail CAV in (36) gives the constraint:

$$L_f h_{\mathrm{T}}(\mathbf{x}) + L_{g_{\mathrm{T}}} h_{\mathrm{T}}(\mathbf{x}) u_{\mathrm{T}} \geq -\gamma_{\mathrm{T}} h_{\mathrm{T}}(\mathbf{x}), \tag{54}$$

with $L_f h_{\mathrm{T}}(\mathbf{x}) = v_{\mathrm{N}} - v_{\mathrm{T}}$, $L_{g_{\mathrm{T}}} h_{\mathrm{T}}(\mathbf{x}) = -\tau_{\mathrm{T}}$, and $\gamma_{\mathrm{T}} > 0$, which is equivalent to:

$$u_{\mathrm{T}} \leq \frac{1}{\tau_{\mathrm{T}}}(v_{\mathrm{N}} - v_{\mathrm{T}}) + \gamma_{\mathrm{T}}\left(\frac{1}{\tau_{\mathrm{T}}} s_{\mathrm{T}} - v_{\mathrm{T}}\right); \tag{55}$$

cf. the ACC terms in (14). The corresponding safety filter that ensures the tail CAV's safety is:

$$k_{\mathrm{T}}(\mathbf{x}) = \min\left\{k_{\mathrm{T,n}}(\mathbf{x}), \frac{1}{\tau_{\mathrm{T}}}(v_{\mathrm{N}} - v_{\mathrm{T}}) + \gamma_{\mathrm{T}}\left(\frac{1}{\tau_{\mathrm{T}}}s_{\mathrm{T}} - v_{\mathrm{T}}\right)\right\}, \tag{56}$$

with the nominal controller $k_{\mathrm{T,n}}$ in (14).

HV safety: When a middle HV-i is connected to the head CAV, the CBF also enables the head CAV to improve the HV's safety. It is noted that here safe motions are enforced by car-following behaviors and therefore the head-CAV control input is constrained to this purpose. We design constraints on the head CAV controller to ensure HV safety as follows. For the HV safety function h_i in (37), we have that $L_g h_i(\mathbf{x}) = \begin{bmatrix}0 & 0\end{bmatrix}$, which means HV's safety measure h_i does not directly constrain any of the control inputs u_{H} or u_{T} due to the relative degree of the system. Thus, we introduce a CBF for HV-i:

$$\bar{h}_i(\mathbf{x}) = h_i(\mathbf{x}) - \eta_i h_{\mathrm{H}}(\mathbf{x}), \tag{57}$$

where $\eta_i > 0$ is a parameter. Then we have $L_g \bar{h}_i(\mathbf{x}) = \begin{bmatrix}\eta_i \tau_{\mathrm{H}} & 0\end{bmatrix}$, which provides a way to constrain the control input u_{H} for safety. By ensuring both $h_{\mathrm{H}}(\mathbf{x}) \geq 0$ and $\bar{h}_i(\mathbf{x}) \geq 0$, we have $h_i(\mathbf{x}) \geq 0$. The safety constraint from $\bar{h}_i$ is then:

$$L_f \bar{h}_i(\mathbf{x}, v_{\mathrm{d}}) + L_{g_{\mathrm{H}}} \bar{h}_i(\mathbf{x}) u_{\mathrm{H}} \geq -\gamma_i \bar{h}_i(\mathbf{x}), \tag{58}$$

with $L_f \bar{h}_i(\mathbf{x}, v_{\mathrm{d}}) = v_{i-1} - v_i - \tau_i F_i(s_i, v_i, v_{i-1} - v_i) - \eta_i(v_{\mathrm{d}} - v_{\mathrm{H}})$, $L_{g_{\mathrm{H}}} \bar{h}_i(\mathbf{x}) = \eta_i \tau_{\mathrm{H}}$, and $\gamma_i > 0$. Thus $\bar{h}_i$ gives a constraint on the head CAV's controller as:

$$u_{\mathrm{H}} \geq \frac{1}{\tau_{\mathrm{H}}}(v_{\mathrm{d}} - v_{\mathrm{H}}) + \gamma_i\left(\frac{1}{\tau_{\mathrm{H}}}s_{\mathrm{H}} - v_{\mathrm{H}}\right) + \frac{\tau_i}{\eta_i \tau_{\mathrm{H}}}\left(F_i(s_i, v_i, v_{i-1} - v_i) - \frac{1}{\tau_i}(v_{i-1} - v_i) - \gamma_i\left(\frac{1}{\tau_i}s_i - v_i\right)\right). \tag{59}$$

While the head CAV safety constraint (52) gives an upper bound on u_{H}, the HV safety condition (59) sets a lower bound on u_{H}. These two bounds may conflict with each other, thus there may be no available controller to enforce the safety of both the head CAV and the HVs. Therefore, we set the head CAV safety as a hard constraint and HV safety as soft constraints by adding a relaxation term to the HV safety constraints. This leads to the following safety filter that ensures the safety of the head CAV while facilitating the safety of HVs:

$$\begin{aligned} k_{\mathrm{H}}(\mathbf{x}, v_{\mathrm{d}}) = \underset{u_{\mathrm{H}} \in \mathbb{R}, \sigma_i \geq 0}{\operatorname{argmin}} \ & \|u_{\mathrm{H}} - k_{\mathrm{H,n}}(\mathbf{x}, v_{\mathrm{d}})\|^2 + \sum_{i=1}^{N} p_i \sigma_i^2 \\ \text{s.t. head CAV safety}: \ & L_f h_{\mathrm{H}}(\mathbf{x}, v_{\mathrm{d}}) + L_{g_{\mathrm{H}}} h_{\mathrm{H}}(\mathbf{x}) u_{\mathrm{H}} \geq -\gamma_{\mathrm{H}} h_{\mathrm{H}}(\mathbf{x}), \\ \text{HV safety}: \ & \begin{cases} L_f \bar{h}_1(\mathbf{x}, v_{\mathrm{d}}) + L_{g_{\mathrm{H}}} \bar{h}_1(\mathbf{x}) u_{\mathrm{H}} \geq -\gamma_1 \bar{h}_1(\mathbf{x}) - \sigma_1, \\ \quad \vdots \\ L_f \bar{h}_N(\mathbf{x}, v_{\mathrm{d}}) + L_{g_{\mathrm{H}}} \bar{h}_N(\mathbf{x}) u_{\mathrm{H}} \geq -\gamma_N \bar{h}_N(\mathbf{x}) - \sigma_N, \end{cases} \end{aligned} \tag{60}$$

where σ_i represent the relaxation term and $p_i > 0$ are penalty parameters for the relaxation. This type of controller was first proposed for a single CAV in Zhao et al. (2023) which was called safety-critical traffic controller. If a HV is not connected to the head CAV, the corresponding HV safety constraint shall be omitted from (60). If no HVs are connected to the head CAV, then all HV safety constraints are dropped, and (60) reduces to (53).

Platoon safety: In the above design, to ensure the safety of each individual HV, the HV is required to connect to the head CAV. If some HVs are non-connected, we propose to enforce *platoon safety* that constrains the overall length of the vehicle platoon, i.e., the total gap between the two CAVs must exceed a minimum value. Since the two CAVs are connected, the gap s_{HT} between them is available. The gap s_{HT} can be expressed by $s_{\mathrm{HT}} = s_{\mathrm{T}} + \sum_{i=1}^{N} s_i + l_{\mathrm{T}} + \sum_{i=1}^{N} l_i$ with l_{T} and l_i being the length of the tail CAV and HV-i, and thus s_{HT} is a function of the system state $\mathbf{x}$. Based on s_{HT}, we define the platoon safety function as:

$$h_{\mathrm{p}}(\mathbf{x}) = s_{\mathrm{HT}} - l_0 - \tau_{\mathrm{p}}(v_{\mathrm{T}} - v_{\mathrm{H}}), \tag{61}$$

where $l_0 > 0$ is the base length of the platoon and $\tau_{\mathrm{p}} > 0$ is a parameter. The safety constraint constructed by h_{p} is:

$$L_f h_{\mathrm{p}}(\mathbf{x}) + L_g h_{\mathrm{p}}(\mathbf{x}) \mathbf{u} \geq -\gamma_{\mathrm{p}} h_{\mathrm{p}}(\mathbf{x}), \tag{62}$$

with $L_f h_{\mathrm{p}}(\mathbf{x}) = v_{\mathrm{H}} - v_{\mathrm{T}}$, $L_g h_{\mathrm{p}}(\mathbf{x}) = \begin{bmatrix}\tau_{\mathrm{p}} & -\tau_{\mathrm{p}}\end{bmatrix}$, and $\gamma_{\mathrm{p}} > 0$. This is equivalent to:

$$u_{\mathrm{T}} - u_{\mathrm{H}} \leq \frac{1}{\tau_{\mathrm{p}}}(v_{\mathrm{H}} - v_{\mathrm{T}}) + \gamma_{\mathrm{p}}\left(\frac{1}{\tau_{\mathrm{p}}}(s_{\mathrm{HT}} - l_0) - (v_{\mathrm{T}} - v_{\mathrm{H}})\right). \tag{63}$$

The platoon safety constraint is of the form $u_{\mathrm{T}} - u_{\mathrm{H}} \leq \bar{u}$ with $\bar{u}$ being the right-hand side of (63). Meanwhile, the safety of the head CAV can be guaranteed by enforcing an upper bound on its control input u_{H} in the form $u_{\mathrm{H}} \leq \bar{u}_{\mathrm{H}}$ where $\bar{u}_{\mathrm{H}}$ is the right-hand side of (52). The tail CAV's safety can be guaranteed by a similar upper bound on its input u_{T} as $u_{\mathrm{T}} \leq \bar{u}_{\mathrm{T}}$ where $\bar{u}_{\mathrm{T}}$ is the right-hand side of (55). Fig. 4 illustrates these input constraints. Depending on the values of $\bar{u}_{\mathrm{H}}$, $\bar{u}_{\mathrm{T}}$, and $\bar{u}$, there are three possible cases, as shown by the three panels. In each case, there exists a feasibility region for the control inputs u_{H} and u_{T} where the safety of the head CAV, tail CAV, and platoon can be enforced simultaneously without relaxation (see shaded domain). This is summarized by the following Lemma.

Lemma 2. *There always exist $u_{\mathrm{H}} \in \mathbb{R}$ and $u_{\mathrm{T}} \in \mathbb{R}$ that satisfy three constraints: head CAV safety (52), tail CAV safety (55), and platoon safety (63), for all $\mathbf{x} \in \mathbb{R}^n$ and $v_{\mathrm{d}} \in \mathbb{R}$.*

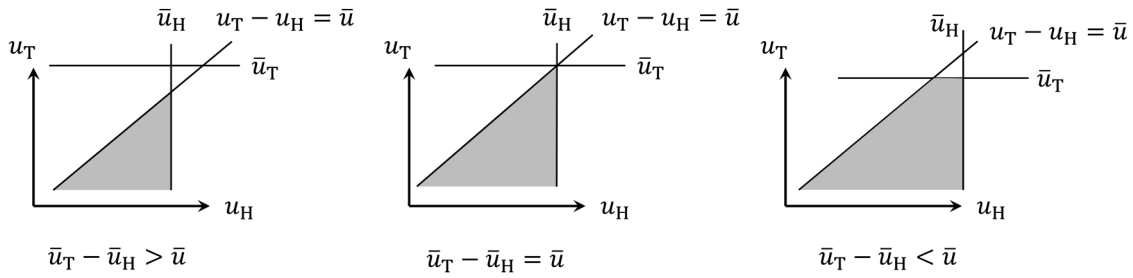

Fig. 4. Region of (u_H, u_T) control inputs that ensure the safety of both the head CAV using (52), the tail CAV using (55), and the platoon using (63).

This finally leads to the following safety filter that ensures CAV safety, HV safety (with relaxation), and platoon safety:

$$
\begin{aligned}
k(\mathbf{x}, v_d) = \underset{\mathbf{u}\in\mathbb{R}^2, \sigma_i \geq 0}{\operatorname{argmin}} \ & \|\mathbf{u} - k_n(\mathbf{x}, v_d)\|^2 + \sum_{i=1}^{N} p_i \sigma_i^2 \\
\text{s.t. CAV safety}: \ & \begin{cases} L_f h_H(\mathbf{x}, v_d) + L_{g_H} h_H(\mathbf{x}) u_H \geq -\gamma_H h_H(\mathbf{x}), \\ L_f h_T(\mathbf{x}) + L_{g_T} h_T(\mathbf{x}) u_T \geq -\gamma_T h_T(\mathbf{x}), \end{cases} \\
\text{HV safety}: \ & \begin{cases} L_f \bar{h}_1(\mathbf{x}, v_d) + L_{g_H} \bar{h}_1(\mathbf{x}) u_H \geq -\gamma_1 \bar{h}_1(\mathbf{x}) - \sigma_1, \\ \quad \vdots \\ L_f \bar{h}_N(\mathbf{x}, v_d) + L_{g_H} \bar{h}_N(\mathbf{x}) u_H \geq -\gamma_N \bar{h}_N(\mathbf{x}) - \sigma_N, \end{cases} \\
\text{Platoon safety}: \ & L_f h_p(\mathbf{x}) + L_g h_p(\mathbf{x}) u \geq -\gamma_p h_p(\mathbf{x}).
\end{aligned}
\tag{64}
$$

It is noted that the platoon safety constraint depends on the inputs of both CAVs. Therefore, when this constraint is enforced, the two control inputs u_H and u_T need to be computed together. If it is infeasible in practice to compute the control inputs of two CAVs jointly, the platoon safety constraint shall be omitted from (64). This leads back to the controller (56) for the tail CAV and the controller (60) for the head CAV which no longer depend on each other. The safety-critical controller (64) is a QP, which can be solved efficiently for real-time application in practical traffic systems. The number of constraints in the QP increases with the number of HVs. Considering the wireless communication range, there may be approximately at most ten HVs between the two CAVs Kuutti et al. (2018), which means a low computation burden to solve the QP.

Remark 10 (Look-ahead for stability and look-behind for safety)**.** As discussed in Remark 3–4 regarding the stability chart in Fig. 2, for string stability, the tail CAV must look ahead and include feedback from either the middle HVs or the head CAV. As for HV safety, the head CAV should look behind and alter its controller using a safety filter based on the states of the HVs.

5. Numerical simulation

In this section, we conduct a number of simulations to validate the safety and performance of the proposed safety-critical controller (64). We first consider the case where no HVs are connected to the CAVs, and we discuss CAV safety in subsection 5.1. Then we consider connected HVs and HV safety in Subsection 5.2. Finally, we demonstrate the behavior of the controller that enforces platoon safety in subsection 5.3.

5.1. CAV Safety guaranteed via CBF

We consider two safety-critical scenarios that may happen in mixed traffic and pose rear-end collision risks:

- *The head HV suddenly decelerates.* This will pose safety risks for the H-CAV, and possibly also for the T-CAV. This may be caused in real traffic by an aggressive cut-in, pedestrian, or obstacles on the road. In the simulation, we set the head HV's acceleration profile as:

$$
\dot{v}_d = \begin{cases} -a_d, & t \in [2, 2 + \Delta v_d / a_d], \\ a_d, & t \in (2 + \Delta v_d / a_d, 2 + 2\Delta v_d / a_d], \\ 0, & \text{otherwise}, \end{cases}
\tag{65}
$$

  where a_d is a constant deceleration, Δv_d is its speed perturbation, and $\Delta v_d / a_d$ is the duration of deceleration.
- *One middle HV suddenly decelerates.* This will pose safety risks for the T-CAV. We make the HV-i suddenly reduce its speed by Δv_i with a constant deceleration a_i. The acceleration profile of HV-i is modified from (5) to:

$$
\dot{v}_i = \begin{cases} -a_i, & t \in [2, 2 + \Delta v_i / a_i], \\ F_i(s_i, v_i, \dot{s}_i), & \text{otherwise}. \end{cases}
\tag{66}
$$

Considering the physical limits of vehicle braking systems, we use saturated acceleration in the simulation, i.e., $\dot{v}_i = \mathrm{sat}(F_i(s_i, v_i, \dot{s}_i))$, $\dot{v}_\mathrm{H} = \mathrm{sat}(u_\mathrm{H})$, $\dot{v}_\mathrm{T} = \mathrm{sat}(u_\mathrm{T})$, where the saturation function is

$$\mathrm{sat}(u) = \begin{cases} u_{\min}, & u < u_{\min}, \\ u, & u_{\min} \le u \le u_{\max}, \\ u_{\max}, & u > u_{\max}, \end{cases} \tag{67}$$

with $u_{\max}$ and $u_{\min}$ being the maximum and minimum acceleration. In the simulation, we use $u_{\max} = 7$ m/s^2 and $u_{\min} = -7$ m/s^2. For the nominal stabilizing controller, we consider CAV coordination gain as $\beta_{\mathrm{H,T}} = 0.5$ s^{-1} and $\beta_{\mathrm{T,H}} = 1.2$ s^{-1}. We set the safe time headway as $\tau_\mathrm{H} = 0.8$ s and $\tau_\mathrm{T} = 0.8$ s. For the CBF parameters, we use $\gamma_\mathrm{H} = 5$ s^{-1} and $\gamma_\mathrm{T} = 5$ s^{-1}. The human-driver model F_i and the rest of the parameters are the same as in Section 3.2.

Fig. 5 shows the simulated trajectories by using the nominal controller (12), (14) and the safety-critical controller (53), (56) for the first scenario when the head HV suddenly decelerates from $v^* = 20$ m/s to a stop with $a_\mathrm{d} = 5$ m/s^2 and $\Delta v_\mathrm{d} = 20$ m/s. The behavior of the nominal controller is shown in the top row. The CAVs stabilize the traffic by having a small deceleration (see panels (c) and (d)), but this causes a collision between the head CAV and the head HV (see the negative gap along the blue curve in panel (b)). Besides, the tail CAV also becomes unsafe in the sense that its safety function becomes negative (see the red curve in panel (a)). The behavior of the safety-critical controller that includes the CBF-based safety filter is shown in the bottom row. Initially, when the head HV drives at the constant speed v^*, the safety-critical controller matches the nominal controller since it satisfies the CBF constraints (52), (55). When the head HV begins to decelerate, the CBF is activated around 5 sec, and the head CAV has a larger deceleration than with the nominal controller (see panels (g) and (h)). This way the head CAV successfully avoids collision (see the positive gap in panel (f)). The safety functions are kept positive throughout the motion (see panel (e)), which indicates that both CAVs are safe.

Besides avoiding unsafe scenarios caused by the nominal controller, the safety-critical controller also maintains both plant stability and head-to-tail string stability of the system. From the profiles of gap s in the second column and speed v in the third column of Fig. 5, we observe plant stability as s and v converge to the equilibrium values s^* and v^* around 45 sec. To evaluate head-to-tail string stability, we quantify the speed perturbations of the tail CAV relative to the head HV by:

$$I = \frac{\sqrt{\int_0^T (v_\mathrm{T} - v^*)^2 \,\mathrm{d}t}}{\sqrt{\int_0^T (v_\mathrm{d} - v^*)^2 \,\mathrm{d}t}}, \tag{68}$$

where $T = 50$ sec is the total simulation length. By Definition 2, if $I < 1$, then the system is head-to-tail string stable. After incorporating the CBF, we have $I = 0.698 < 1$. Therefore, by implementing CBF, the system is both string stable and safe. Note that $I = 0.589$ for the nominal controller, i.e., the value of I is higher for the safety-critical controller. This means that safety is achieved at the price of higher speed fluctuations (but without losing head-to-tail string stability).

In Fig. 6, we plot the profiles of the safety function, gap, speed, and acceleration when one middle HV suddenly decelerates. We consider HV-4 to decelerate with $a_4 = 5$ m/s^2 and $\Delta v_4 = 20$ m/s. As the top row of Fig. 6 shows, when using the nominal controller (12), (14), the deceleration of HV-4 poses a safety risk for the tail CAV. Meanwhile, based on the bottom row, the safety-critical controller (53), (56) with the CBF has a larger deceleration for the tail CAV to avoid collisions. In this scenario, the safety-filtered controller still stabilizes, since the system converges to the equilibrium state after the perturbation of HV-4 (around 40 sec). We note that the head-to-tail string stability index in (68) is not applicable, since it concerns cases where the head HV has a speed perturbation while in this scenario the head HV drives at a constant speed.

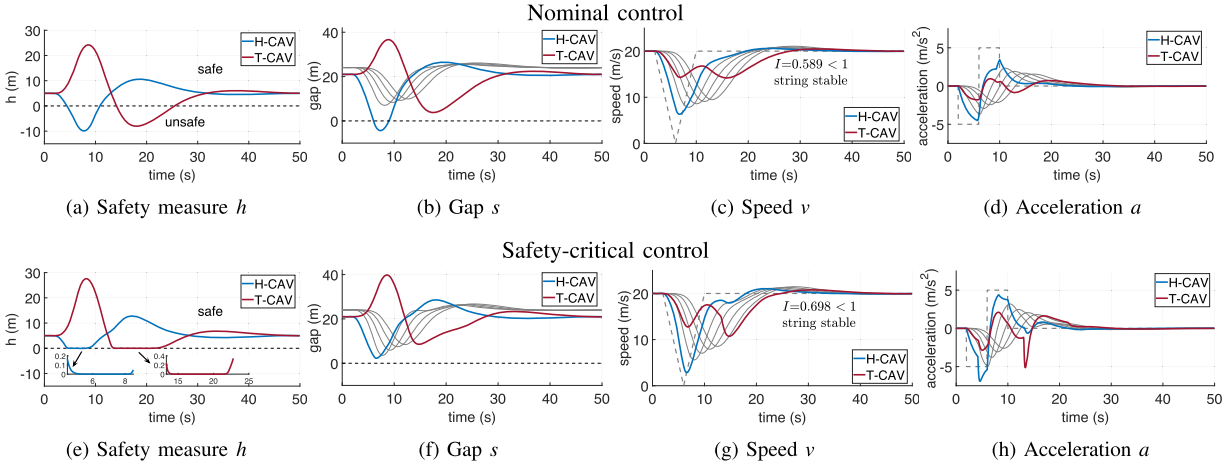

(a) Safety measure h (b) Gap s (c) Speed v (d) Acceleration a

(e) Safety measure h (f) Gap s (g) Speed v (h) Acceleration a

Fig. 5. *The head HV suddenly decelerates:* simulated trajectory of the mixed vehicle platoon. The nominal controllers (12), (14) cause unsafe driving for the two CAVs, i.e., $h_\mathrm{H} < 0$ and $h_\mathrm{T} < 0$ occur. By using the proposed safety-critical controllers (53), (56) with CBF, the two CAVs become safe with positive h_H, h_T. Besides, string stability is also maintained, i.e., $I < 1$.

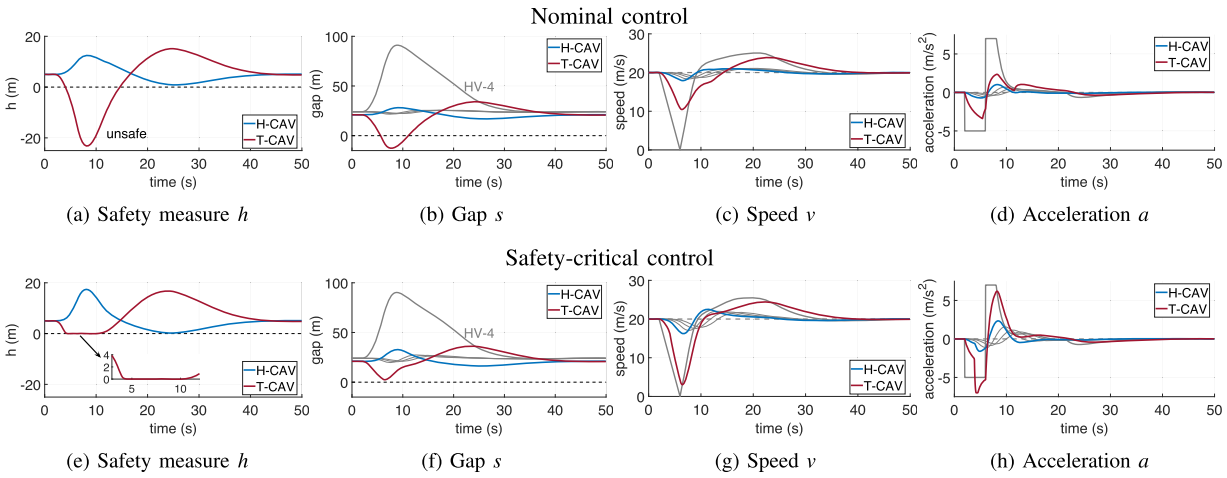

(a) Safety measure h (b) Gap s (c) Speed v (d) Acceleration a

(e) Safety measure h (f) Gap s (g) Speed v (h) Acceleration a

Fig. 6. *A middle HV suddenly decelerates:* simulated trajectory of the mixed vehicle platoon. Due to the deceleration of HV-4, the tail CAV becomes unsafe when using the nominal controller, while the CBF guarantees safety.

5.2. Connected HV safety and effect of HV connection

If a middle HV is connected to the head CAV, then the head CAV may facilitate the safety of this HV via the CBF constraint in (58). We validate this HV safety constraint. We consider a scenario where *one middle HV suddenly accelerates*. This increases the collision risk between the accelerating HV and its leader. We set HV-i to suddenly accelerate with the acceleration profile:

$$\dot{v}_i = \begin{cases} a_i, & t \in [2, 2 + \Delta v_i/a_i], \\ F_i(s_i, v_i, \dot{s}_i), & \text{otherwise}, \end{cases} \tag{69}$$

with a_i being a constant acceleration, and Δv_i being the speed perturbation. We assume that the accelerating HV is HV-1, which is connected to the head CAV, and the nominal controller of the head CAV (12) includes HV-1's feedback with the controller gain $\beta_{\mathrm{H},1} = 0.1$. The corresponding safety-critical controller of the head CAV is given by (60), where the HV-1 safety constraint with $\bar{h}_1$ is included while the other HV safety constraints are omitted. We set the HV's safe time headway as $\tau_1 = 1$ s, and the CBF parameters as $\gamma_1 = 5\ \mathrm{s}^{-1}$, $\eta_1 = 0.5$, $p_1 = 100$. Other parameters, including the tail CAV's nominal controller (14) and safety-critical controller (56), the saturation function, and the CBF parameters for the head and tail CAVs, remain the same.

Fig. 7 plots the trajectories by the nominal controller (12), (14) and the safety-critical controller (56), (60) with $a_1 = 5\ \mathrm{m/s}^2$ and $\Delta v_1 = 3.5$ m/s. The results with the nominal controller are shown in the top row. When HV-1 suddenly accelerates, the head CAV also accelerates, but the gap between HV-1 and the head CAV still becomes too small, hence HV-1 is unsafe (see negative h_1). By using the CBF, as shown in the bottom row, the head CAV generates a larger acceleration. This enlarges the gap between HV-1 and the head CAV, and thus ensures safety (i.e., h_1 is positive for all time). In this scenario, the safety-filtered controller still stabilizes, since the system converges to the equilibrium state around 25 sec.

Connectivity of HVs: Next, we investigate how the connectivity of HVs to CAVs affects the stability and safety of the nominal controller. These simulations correspond to the stability results presented earlier in Fig. 2, which considered three communication topologies: no HV connection, tail CAV connects to HVs (look ahead), and head CAV connects to HVs (look behind). We investigate the behavior of the vehicle platoon for each communication topology in three simulation scenarios: head HV decelerates, middle HV decelerates, and middle HV accelerates; corresponding to Figs. 5, 6 and 7.

The simulation results are shown in Fig. 8, where the top row presents the tail CAV's speed, the bottom row shows the tail CAV's safety function, while the three columns correspond to the three simulation scenarios. Note that the safety functions of the head CAV and middle HVs yield similar curves for each case, thus these plots are omitted. We see that for all three scenarios looking behind has a marginal effect on the results. At the same time, the tail CAV has a smoother speed by looking ahead, which reduces perturbations for the upstream traffic. However, the tail CAV also has a higher risk for unsafe behavior by looking ahead (i.e., the minimum of h_{T} becomes smaller) compared to the case of no HV connection. This can be remedied by using CBF-based safety filters, as it was demonstrated in Fig. 5.

5.3. Platoon safety

Finally, we investigate platoon safety, which requires that the gap between the two CAVs is greater than a safe minimum value. While platoon safety does not refer to collision-based safety for a single vehicle, it prevents the gap between the two CAVs from becoming too small and increases the safety of the overall platoon. On the other hand, this also enhances the stability of traffic flow. To demonstrate this, we run simulations with the safety-critical controller (64) that enforces platoon safety (while we omit the HV safety constraints). We consider the scenario of Fig. 5 where the head HV decelerates. We set the vehicle length as $l_i = 5$ m, and the

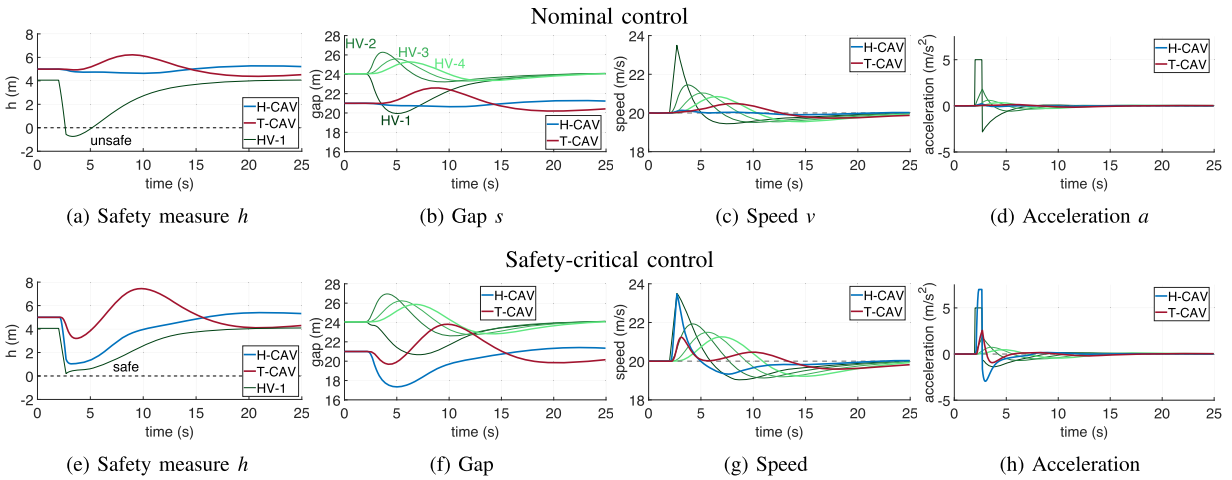

(a) Safety measure h (b) Gap s (c) Speed v (d) Acceleration a

(e) Safety measure h (f) Gap (g) Speed (h) Acceleration

Fig. 7. *A middle HV suddenly accelerates:* simulated trajectory of the mixed vehicle platoon. The safety-critical controller (56), (60) with the CBF guides the head CAV to accelerate so that collision between HV-1 and the head CAV is avoided.

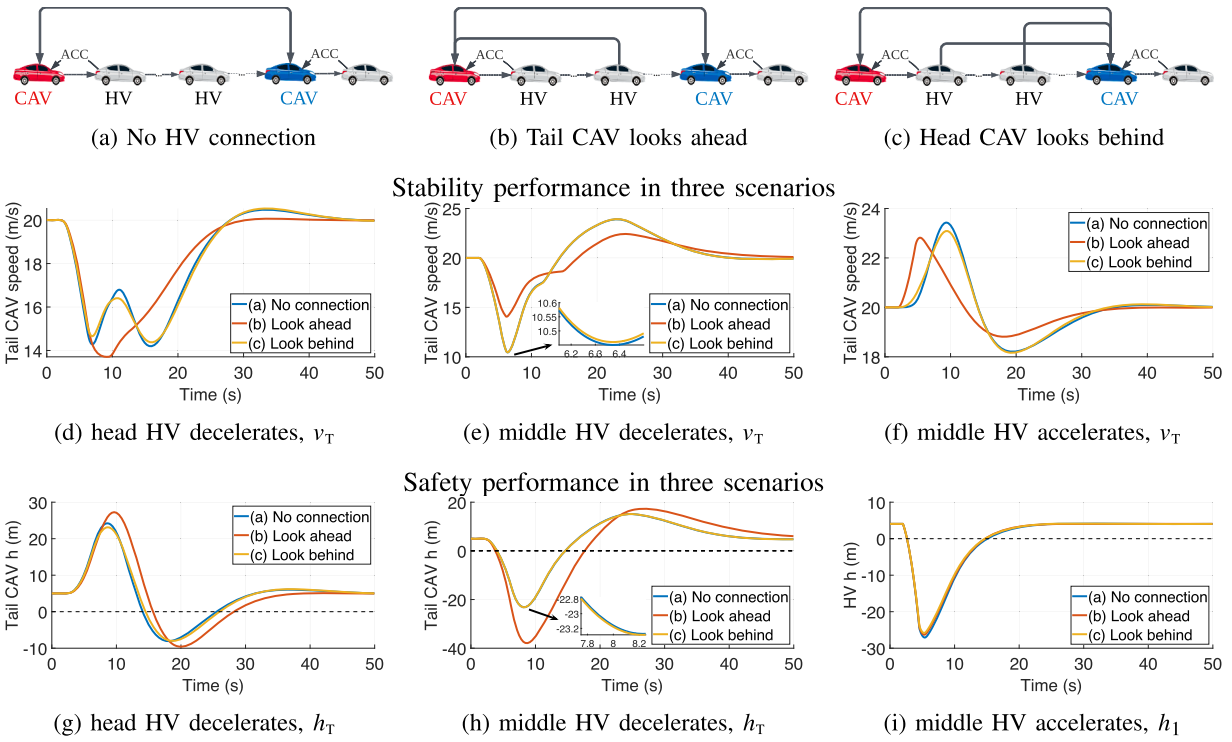

(a) No HV connection (b) Tail CAV looks ahead (c) Head CAV looks behind

(d) head HV decelerates, v_{T} (e) middle HV decelerates, v_{T} (f) middle HV accelerates, v_{T}

(g) head HV decelerates, h_{T} (h) middle HV decelerates, h_{T} (i) middle HV accelerates, h_1

Fig. 8. Simulations of the nominal controller demonstrating the effect of HV connection on stability (first row) and safety (second row). When the tail CAV connects to HVs (look ahead), it reduces its speed fluctuations but also hinders its safety compared to the case of no connection. When the head CAV connects to HVs (look behind), it has a marginal effect.

regular length of the vehicle platoon as $l_0 = 100$ m. We use $\tau_{\mathrm{p}} = 1$ s and $\gamma_{\mathrm{p}} = 5$ s^{-1} to enforce platoon safety. All other parameters remain the same as in Fig. 5.

Fig. 9 plots the simulated trajectories. Compared with the trajectories in Fig. 5, we see that the string stability index in Fig. 9 is reduced from 0.698 to 0.679, indicating that the tail CAV has smaller speed perturbations. Furthermore, the maximum deceleration of the tail CAV is -5 m/s^2 when platoon safety is not enforced (see Fig. 5(h)), while it is only -4 m/s^2 by enforcing platoon safety (see Fig. 9(d)). This is because the tail CAV begins to decelerate earlier when it intends to maintain platoon safety, which results in milder deceleration and smoother motion.

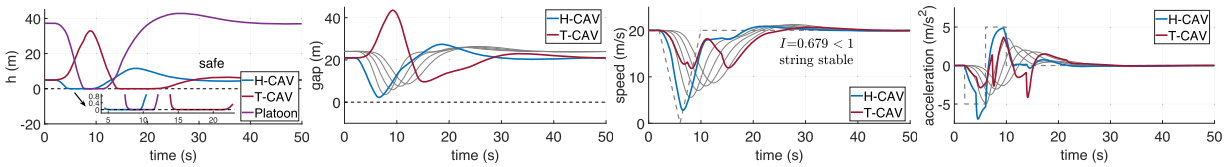

(a) Safety function h (b) Gap (c) Speed (d) Acceleration

Fig. 9. Simulated trajectories when the head HV suddenly decelerates and platoon safety is enforced by the two CAVs. Enforcing platoon safety helps reduce the deceleration of the tail CAV compared to the case without platoon safety (Fig. 5).

6. Performance analysis

The main simulation results have validated that the proposed cooperative CAV controllers achieve both stability and safety, and, therefore, provide an improvement over the nominal control design. We further analyze the performance of the controllers for a wide range of parameters in this section and discuss the sensitivity and robustness of our design with respect to uncertain human driver behaviors.

6.1. Comparison between different CAV control strategies

First, we compare the proposed CAV pair controller to mixed traffic controllers that have been designed with only one head CAV: leading cruise control (LCC) from Wang et al. (2022) and safety-critical traffic control (STC) from our previous work Zhao et al. (2023). We show stability and safety improvement brought by the CAV pair. We run simulations for LCC and STC under the setting of Fig. 5, with the only difference that the tail CAV is replaced by a connected tail HV (i.e., the vehicle chain contains one head CAV and five following HVs). For stability evaluation, we use the stability index I defined in (68). A lower I implies less speed perturbation and more stable traffic. To evaluate safety, we define the safety index as:

$$H = \int_0^T \min\{h(\mathbf{x}(t)), 0\}\, \mathrm{d}t. \tag{70}$$

$H = 0$ implies that the system remains safe, i.e., $h(\mathbf{x}(t)) \geq 0$. For a negative H, its value reflects the extent and duration of the system being unsafe. We compare the safety index and stability index in Table 1. Compared with LCC, the designed nominal controller (12), (14) enhances both traffic stability and safety. Comparing STC with the proposed safety-critical controller (53), (56), while they both guarantee system safety, the pair CAV controller has a lower speed perturbation.

6.2. Trade-offs between stability and safety

Next, we consider the safety-critical controllers (53), (56) that enforce CAV safety only. We further investigate the effects of safety filters on safety and stability by conducting simulations with various control gains $(\beta_{\mathrm{H,T}}, \beta_{\mathrm{T,H}})$, considering the scenario where the head HV suddenly decelerates. That is, the simulations in Fig. 5 are repeated with different gains.

Effect of CBF on safety

In theory, the safety-critical controllers guarantee safety with any nominal controller and in all scenarios. However, safety guarantees hold for unbounded accelerations only. If the CBF requires too large acceleration or deceleration, the CAV's control input is saturated, and safety guarantees could be lost. We analyze how the nominal controller and the safety-critical controller affect the two CAVs' safety with saturated accelerations.

Fig. 10 presents simulation results with various controller gains $(\beta_{\mathrm{H,T}}, \beta_{\mathrm{T,H}})$. The first and second columns plot the maximum speed perturbation Δv_{d} of the head HV for which the head and tail CAV remain safe. A darker color indicates that the CAV is able to maintain safety at larger speed perturbations. Fig. 10(b) and (f) show that, by adding the CBF-based safety filters, both the head and tail CAV remain safe for almost all controller gains even when the head HV decelerates to a full stop, i.e., $\Delta v_{\mathrm{d}} = 20$ m/s. The third and fourth columns present the range of controller gains $(\beta_{\mathrm{H,T}}, \beta_{\mathrm{T,H}})$ that ensure the safety of the head and tail CAVs for a fixed speed perturbation Δv_{d}. Fig. 10(c) and (g) give the safety region for $\Delta v_{\mathrm{d}} = 12$ m/s. As the grey area shows, the nominal controller can

Table 1
Stability and safety performance comparison between different CAV control strategies.

	One Head CAV		CAV Pair	
	Leading cruise control Wang et al. (2022)	Safety-critical traffic control Zhao et al. (2023)	Nominal control (12), (14)	Safety-critical control (53), (56)
Safety index H (m·s)	−66.82	0	−38.21	0
Stability index I	0.810	0.882	0.589	0.698

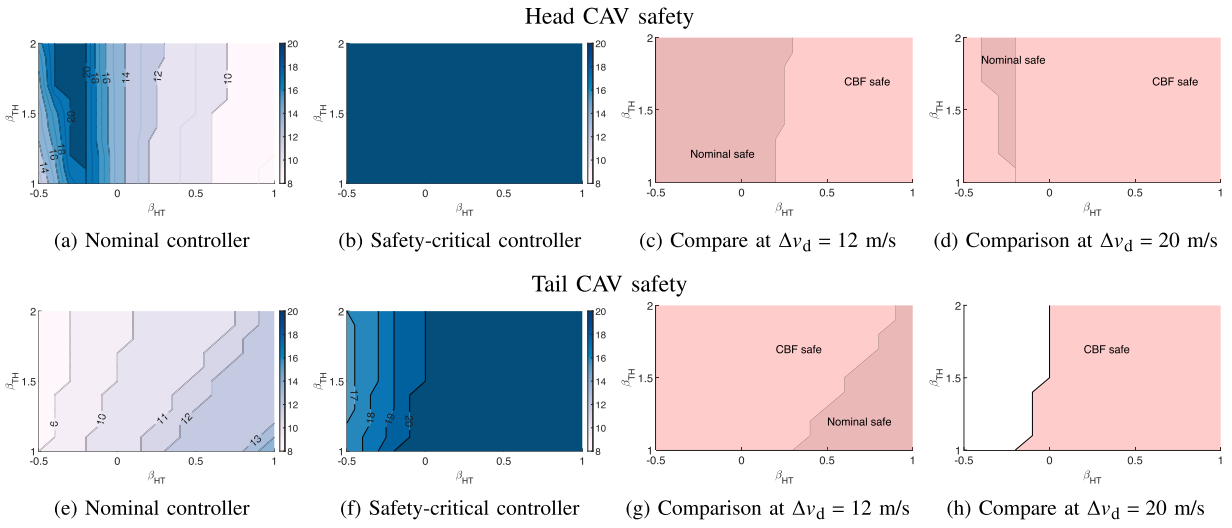

(a) Nominal controller (b) Safety-critical controller (c) Compare at $\Delta v_d = 12$ m/s (d) Comparison at $\Delta v_d = 20$ m/s

(e) Nominal controller (f) Safety-critical controller (g) Comparison at $\Delta v_d = 12$ m/s (h) Compare at $\Delta v_d = 20$ m/s

Fig. 10. Safety performance of the nominal controller and the safety-critical controller with CBF. The first and second rows give results for the head and tail CAV, respectively. The first and second columns show the maximum speed perturbation Δv_d for the head HV so that the CAV remains safe by using the nominal controller and the CBF, respectively, considering various controller gains $(\beta_{H,T}, \beta_{T,H})$. The third and fourth columns provide the range of controller gains under which the CAV is safe for a fixed speed perturbation Δv_d. The grey and red areas correspond to the nominal and safety-critical controller, respectively. (For interpretation of the references to colour in this figure legend, the reader is referred to the web version of this article.)

achieve safety for one of the CAVs with a limited choice of gains. However, by comparing panels (c) and (g), it can be concluded that no gains can enable the nominal controller to ensure safety for both CAVs. As opposed, by adding the CBF-based safety filters, both the head and tail CAVs remain safe for all considered $(\beta_{H,T}, \beta_{T,H})$ gains, as the red region shows. Fig. 10(d) and (h) give the safety region for $\Delta v_d = 20$ m/s. We note from Fig. 10(h) that all nominal controllers fail to ensure the safety of the tail CAV (i.e., there is no grey region), while the CBF still guarantees its safety for most $(\beta_{H,T}, \beta_{T,H})$ pairs (see the red region). The unsafe domain (white region) is caused by the saturation of accelerations.

Effect of CBF on stability

As trajectories in Figs. 5, 6, and 7 show, the CBF may increase the acceleration or deceleration of CAVs to avoid collisions, i.e., there is a trade-off between safety and stability. To evaluate the CBF's effect on string stability (traffic smoothness), we run simulations when the head HV decelerates (i.e., for the scenario of Fig. 5), and we calculate the head-to-tail string stability index I defined in (68). Fig. 11(a) and (b) depict the stability index obtained for the nominal and safety-critical controllers using various $(\beta_{H,T}, \beta_{T,H})$ controller gains. We see that after adding the CBF, we still have $I < 1$ for all gains. Thus, combining the safe region in Fig. 10 and the stability index in Fig. 11, we can conclude that the safety-critical controller (53), (56) achieves both safety and head-to-tail string stability.

Besides evaluating head-to-tail string stability which characterizes the smoothness of the tail CAV's motion, we also investigate the smoothness of the overall mixed traffic considering all vehicles in the platoon. We define the average string stability index:

$$\bar{I} = \frac{1}{N+2}\left(\frac{\sqrt{\int_0^T (v_H - v^*)^2 \, dt}}{\sqrt{\int_0^T (v_d - v^*)^2 \, dt}} + \frac{\sqrt{\int_0^T (v_T - v^*)^2 \, dt}}{\sqrt{\int_0^T (v_d - v^*)^2 \, dt}} + \sum_{i=1}^{N} \frac{\sqrt{\int_0^T (v_i - v^*)^2 \, dt}}{\sqrt{\int_0^T (v_d - v^*)^2 \, dt}} \right). \tag{71}$$

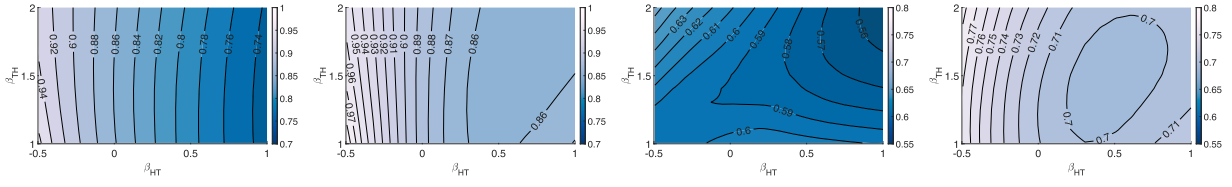

(a) Nominal controller, I (b) Safety-critical controller, I (c) Nominal controller, $\bar{I}$ (d) Safety-critical controller, $\bar{I}$

Fig. 11. Stability performance of the nominal controller and the safety-critical controller with CBF. The first and second columns show the head-to-tail string stability index I defined in (68). A smaller I implies that the tail CAV has smaller speed perturbation, and thus the upstream traffic is smoother. With $I < 1$, the mixed traffic system is considered head-to-tail string stable. The third and fourth columns depict the average string stability index $\bar{I}$ defined in (71). A smaller $\bar{I}$ reflects that the entire mixed vehicle platoon drives more smoothly on average. A darker color implies a smaller I or $\bar{I}$ and thus a smoother traffic.

Fig. 11(c) and (d) plot $\bar{I}$ for the nominal controller and the safety-critical controller. Similar to the head-to-tail string stability index I, the average string stability index $\bar{I}$ becomes higher when implementing CBFs, since the acceleration becomes larger to maintain safety. Nevertheless, we still have $\bar{I} < 1$ for the safety-critical controller, which implies that perturbations from the downstream traffic are attenuated by the platoon of two CAVs and N middle HVs.

6.3. Sensitivity to the CAV penetration rate

We analyze how the number of middle HVs, N, affects the performance of the CAV controllers. Namely, how the CAV penetration rate affects the stability and safety of mixed traffic. We repeat the simulations for the case where the head HV decelerates as in Fig. 5, considering various N values ranging from 1 to 10, with the corresponding penetration rate $p = 2/(N+2)$ ranging from 67 % to 17 %. Note that the vehicle-to-vehicle communication connecting the two CAVs has a limited range, and 10 middle HVs is approximately the maximum N that can be covered by the communication range. Since the middle HVs are assumed to be non-connected, the two CAVs do not respond to them, and the controller remains the same for different numbers of middle HVs. We set all parameters except N to be the same as in Fig. 5.

Fig. 12 shows the simulation results. The first row of Fig. 12 depicts the profiles of speed v_{H}, v_{T} under the nominal controller and the safety-critical controller. We see that the nominal controller stabilizes the system for each N, i.e., the system state converges to the equilibrium once the head HV drives at the equilibrium speed v^*. With more middle HVs, however, it takes more time to converge: the system gets close to the equilibrium around 20 sec for $N = 1$, while it takes 40 sec for $N = 10$. As for string stability, Fig. 12(e) plots the string stability index I as a function of N. We observe that $I < 1$ for all N, i.e., the nominal controller achieves head-to-tail string stability. With the increase of N, I first decreases and then increases. This means that the tail CAV performs best if the head CAV is a few vehicles ahead ($N \approx 4$), which is consistent with the findings in connected cruise control Orosz (2016). When the safety filter is implemented, the effect of the HV number on stability is similar. From Fig. 12(b) and (d), the safety-critical controller still ensures plant stability, i.e., v converges to v^*. As for string stability, as Fig. 12(e) shows, we still have $I < 1$ for all N, which means the system is still head-to-tail string stable with the CBF.

As for safety, we plot h_{H} and h_{T} in the second row of Fig. 12. For the nominal controller, both the head and tail CAV become more unsafe when there are more middle HVs (i.e., the minimum of h becomes smaller as N increases and h goes below zero in each case in Fig. 12(f) and (h)). For the safety-critical controller, as Fig. 12(g) and (i) show, both the head CAV and tail CAV maintain safety in the sense that $h_{\mathrm{H}} \geq 0$ and $h_{\mathrm{T}} \geq 0$. To summarize, by implementing CBF constraints, the mixed vehicle platoon achieves safe and string stable driving.

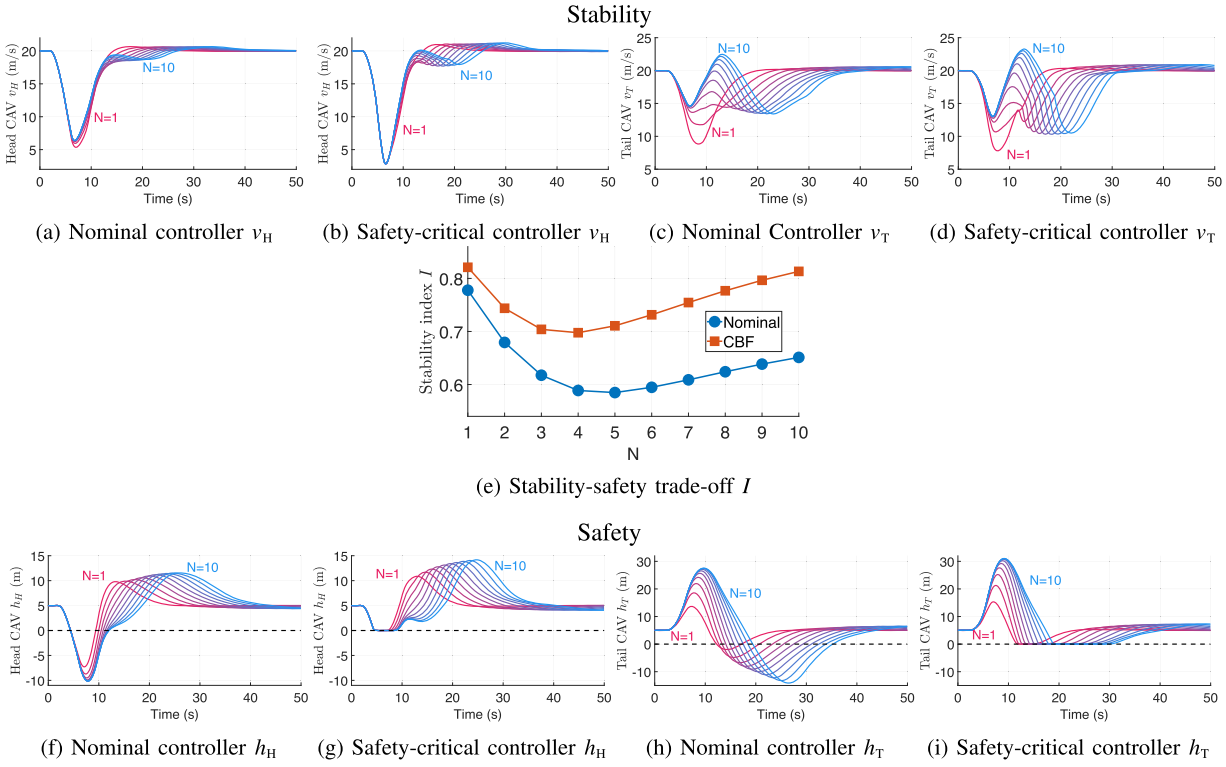

(a) Nominal controller v_{H} (b) Safety-critical controller v_{H} (c) Nominal Controller v_{T} (d) Safety-critical controller v_{T}

(e) Stability-safety trade-off I

(f) Nominal controller h_{H} (g) Safety-critical controller h_{H} (h) Nominal controller h_{T} (i) Safety-critical controller h_{T}

Fig. 12. Simulated trajectories with different numbers of middle HVs, N. The proposed controller achieves both safe ($h \geq 0$) and string stable ($I < 1$) driving for all considered N.

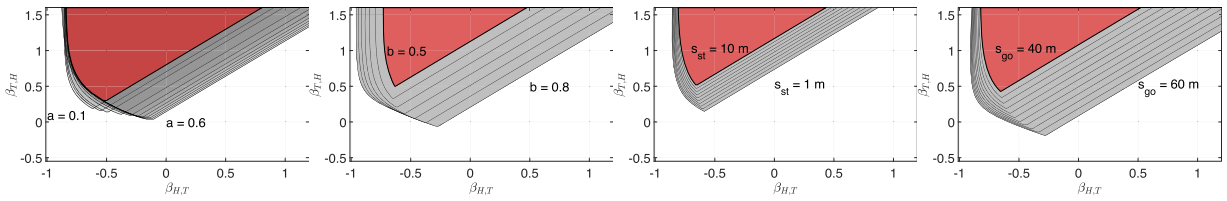

(a) a (b) b (c) s_{st} (d) s_{go}

Fig. 13. Stability charts under different HV model parameters a, b, s_{st}, and s_{go}. In each subfigure, we plot the stability boundaries when one parameter changes with the other three parameters fixed. Each line gives a boundary of head-to-tail string stability for a given parameter value. Each grey area shades the range of $(\beta_{\text{H,T}}, \beta_{\text{T,H}})$ gains that lead to string stability for the corresponding HV model parameter values. The red region is the overlap of string stability regions with varying parameters. (For interpretation of the references to colour in this figure legend, the reader is referred to the web version of this article.)

6.4. Robustness to uncertainty of human driver behaviors

Finally, we study how the proposed controllers are affected by the uncertainty induced by human driver behaviors.

6.4.1. Robust stability with parameter uncertainty in the human driver models

We analyze how the stability performance of the nominal controller is affected by the parameters of the human driver model. We consider the case where the two CAVs are connected only to each other, and repeat the stability calculations in Fig. 2(a) with various HV parameters. There are four parameters in the human driver model (30): sensitivity to desired speed a, sensitivity to leader's speed b, stopping gap s_{st}, and free-driving gap s_{go}. We have found that the plant stability boundaries only have small changes with different HV model parameters. We depict the head-to-tail string stability region with different HV parameters in Fig. 13. In each subfigure, we plot the string stability boundaries when one parameter changes while keeping the other three parameters the same as calibrated in Section 3.3. The overlap between the string stable regions associated with different HV parameters is shaded in red. The red domain shows that there exists a large region of nominal controller gains that renders the system string stable even when the human driver behavior is uncertain. Choosing gains from this region, therefore, provides robustness against human driver uncertainty.

6.4.2. Robust safety with inaccurate human driver model

Finally, we study how safety can be guaranteed when the behavior of human drivers is uncertain. We note that the safety constraints of the head CAV (52), tail CAV (55), and platoon (63) do not depend on the human driver model. Therefore, CAV safety and platoon

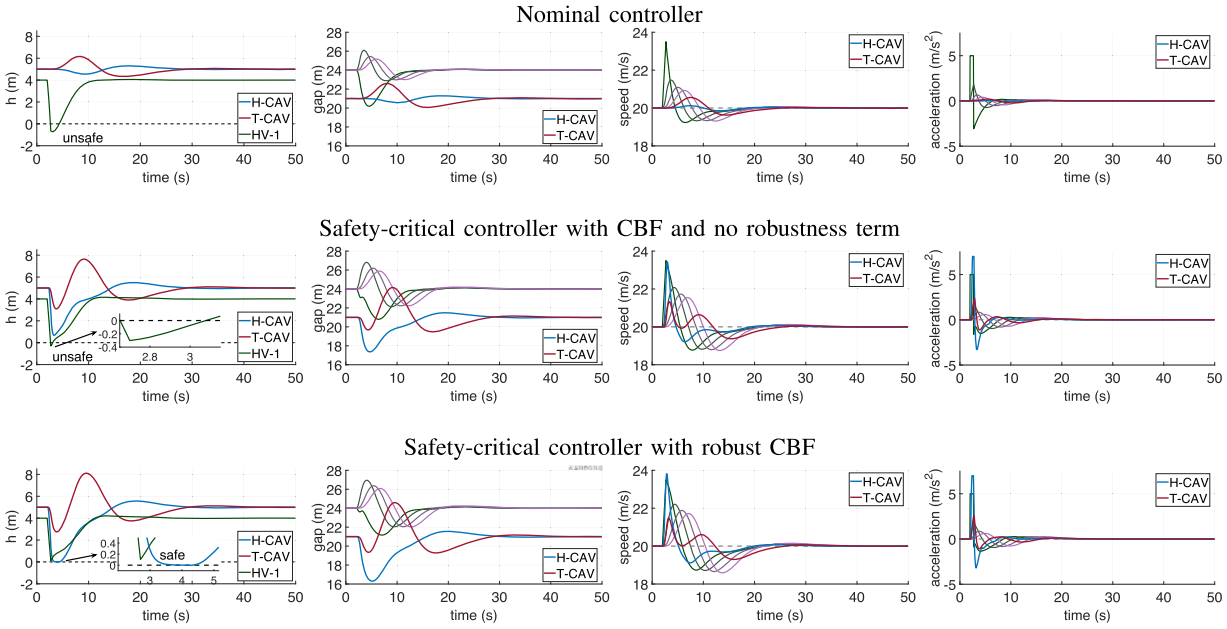

Fig. 14. Simulated trajectories when one middle HV suddenly accelerates. When the human driver model used by the head CAV's control design is inaccurate, the CBF may fail to ensure HV safety. This can be remedied by using a robust CBF that accounts for the human driver uncertainty.

safety can be enforced even if the human-driver model is unknown or inaccurate. The human driver uncertainty only affects the HV safety (59). Below we outline a method to provide robust safety guarantees for HVs even with uncertain human driver model.

Recall that the uncertainty of the human driver model can be captured by a disturbance d_i in (5) that represents the error between the actual acceleration $\dot{v}_i$ and its model F_i. If the disturbance has a known upper bound $\bar{d}_i$, i.e., $|d_i| = |\dot{v}_i - F_i(s_i, v_i, \dot{s}_i)| \le \bar{d}_i$, then the HV safety constraint (58) can be modified based on robust CBF theory Jankovic (2018) to the robust constraint:

$$L_f \bar{h}_i(\mathbf{x}, v_d) + L_{g_H} \bar{h}_i(\mathbf{x}) u_H - \tau_i \bar{d}_i \ge -\gamma_i \bar{h}_i(\mathbf{x}). \tag{72}$$

This leads to safety guarantees for HVs even with model uncertainty, which are established in Theorem 5 in Appendix B.

We validate this robust CBF by simulations for the scenario of one middle HV suddenly accelerating. We compare simulations with the nominal controller (12), (14); the safety-critical controller (56), (60); and the robust safety-critical controller where the constraints in (60) are replaced by (72). We take the calibrated HV model F_i from the previous simulations in Fig. 7, and we use this model to calculate the left-hand side of the safety constraint (58) and the robust safety constraint (72). Then, we simulate the vehicle platoon considering HVs with different parameters: $a = 0.2$, $b = 0.6$, $s_{st} = 8$ m, and $s_{go} = 40$ m. The remaining simulation parameters, including the nominal controller gains, CBF parameters, and HV acceleration settings, are the same as in Fig. 7. Fig. 14 shows the simulated trajectories by the nominal controller, CBF constraint (58), and robust CBF constraint (72) with $\bar{d}_i = 5$ m/s^2. The robust CBF maintains HV safety, while the other two controllers fail to do so.

7. Conclusion

In this paper, we coordinate a pair of CAVs traveling amongst HVs in mixed traffic. Feedback controllers are designed for the two CAVs to utilize CAV cooperation and, possibly, connected HV feedback. Stability and safety conditions are derived for the controller gains, and the effect of CAV coordination and HV connection on stability and safety is analyzed. We find that both CAV coordination and HV connection have opposite effects on stability and safety: including CAV cooperation or HV connection makes it easier to stabilize traffic but harder to maintain safety. To overcome this trade-off, safety filters are designed using control barrier functions considering CAV safety, HV safety, and platoon safety. The controller performance is analyzed via numerical simulations. With the proposed controller, the mixed vehicle platoon travels safely and also mitigates perturbations from downstream traffic. Future extensions of this research include designing robust controllers under V2V communication failure, considering lateral movement, and evaluating the controller from more perspectives such as comfort and fuel consumption.

CRediT authorship contribution statement

Chenguang Zhao: Writing – original draft, Methodology, Validation, Investigation; **Tamas G. Molnar:** Methodology, Writing – review & editing, Investigation; **Huan Yu:** Writing – review & editing, Methodology, Supervision, Investigation, Conceptualization, Funding acquisition.

Appendix A. Stability Analysis

This Appendix provides the mathematical background required for the stability analysis in Section 3, including the derivation of the linearized dynamics in (19) and the corresponding head-to-tail transfer function G.

A.1. Linearized dynamics

We first derive the linearized dynamics (19). Considering the perturbations around the equilibrium as in (18), the dynamics are as follows. For middle HV-i, by linearizing (4)–(5), we obtain:

$$\dot{\tilde{s}}_i = \tilde{v}_{i-1} - \tilde{v}_i, \tag{A.1}$$

$$\dot{\tilde{v}}_i = a_{i1}\tilde{s}_i - a_{i2}\tilde{v}_i + a_{i3}\tilde{v}_{i-1}, \tag{A.2}$$

where the coefficients are $a_{i1} = \frac{\partial F_i}{\partial s_i}(s_i^*, v^*, 0)$, $a_{i2} = \frac{\partial F_i}{\partial \dot{s}_i}(s_i^*, v^*, 0) - \frac{\partial F_i}{\partial v_i}(s_i^*, v^*, 0)$, and $a_{i3} = \frac{\partial F_i}{\partial \dot{s}_i}(s_i^*, v^*, 0)$. For the head CAV, the linearization of (6)–(7) leads to:

$$\dot{\tilde{s}}_H = \tilde{v}_d - \tilde{v}_H, \tag{A.3}$$

$$\dot{\tilde{v}}_H = \xi_H \tilde{s}_H - \eta_H \tilde{v}_H + \beta_{H,d}\tilde{v}_d + \sum_{i \in \mathcal{N}_H} \beta_{H,i}\tilde{v}_i + \beta_{H,T}, \tag{A.4}$$

with $\xi_H = \alpha_H V_H'(s_H^*)$ and $\eta_H = \alpha_H + \beta_{H,d} + \sum_{i \in \mathcal{N}_H} \beta_{H,i} + \beta_{H,T}$. For the tail CAV, linearizing (8)–(9) yields:

$$\dot{\tilde{v}}_T = \tilde{s}_N - \tilde{s}_T, \tag{A.5}$$

$$\dot{\tilde{v}}_T = \xi_T \tilde{s}_T - \eta_T \tilde{v}_T + \beta_{T,N}\tilde{v}_N + \sum_{i \in \mathcal{N}_T} \beta_{T,i}\tilde{v}_i + \beta_{T,H}\tilde{v}_H, \tag{A.6}$$

with $\xi_T = \alpha_T V_T'(s_T^*)$ and $\eta_T = \alpha_T + \beta_{T,N} + \sum_{i \in \mathcal{N}_T} \beta_{T,i} + \beta_{T,H}$.

The linearized dynamics can be written compactly as system (19), where the matrices A and B are:

$$A = \begin{bmatrix} 0 & -1 & 0 & 0 & 0 & 0 & \cdots & 0 & 0 & 0 & 0 \\ \xi_{\mathrm{H}} & -\eta_{\mathrm{H}} & 0 & \beta_{\mathrm{H},1} & 0 & \beta_{\mathrm{H},2} & \cdots & 0 & \beta_{\mathrm{H},\mathrm{N}} & 0 & \beta_{\mathrm{H},\mathrm{T}} \\ 0 & 1 & 0 & -1 & 0 & 0 & \cdots & 0 & 0 & 0 & 0 \\ 0 & a_{13} & a_{11} & -a_{12} & 0 & 0 & \cdots & 0 & 0 & 0 & 0 \\ 0 & 0 & 0 & 1 & 0 & -1 & \cdots & 0 & 0 & 0 & 0 \\ 0 & 0 & 0 & a_{23} & a_{21} & -a_{22} & \cdots & 0 & 0 & 0 & 0 \\ & & & & & & \ddots & & & & \\ 0 & 0 & 0 & 0 & 0 & 0 & \cdots & 0 & 1 & 0 & -1 \\ 0 & \beta_{\mathrm{T},\mathrm{H}} & 0 & \beta_{\mathrm{T},1} & 0 & \beta_{\mathrm{T},2} & \cdots & 0 & \beta_{\mathrm{T},\mathrm{N}} & \xi_{\mathrm{T}} & -\eta_{\mathrm{T}} \end{bmatrix}, \quad B = \begin{bmatrix} 1 \\ \beta_{\mathrm{H,d}} \\ 0 \\ 0 \\ 0 \\ \vdots \\ 0 \\ 0 \end{bmatrix}. \tag{A.7}$$

A.2. Derivation of the transfer function

We derive the head-to-tail transfer function $G(s)$ as follows. For each middle HV-i, we take the Laplace transform of the linearized dynamics (A.1)–(A.2) considering zero initial conditions:

$$s\widetilde{S}_i = \widetilde{V}_{i-1} - \widetilde{V}_i, \tag{A.8}$$

$$s\widetilde{V}_i = a_{i1}\widetilde{S}_i - a_{i2}\widetilde{V}_i + a_{i3}\widetilde{V}_{i-1}, \tag{A.9}$$

where $\widetilde{S}$ and $\widetilde{V}$ denote the Laplace transforms of $\tilde{s}$ and $\tilde{v}$ (with the corresponding subscript). This gives the relationship between $\widetilde{V}_{i-1}$ and $\widetilde{V}_i$ as:

$$\widetilde{V}_i = \frac{a_{i3}s + a_{i1}}{s^2 + a_{i2}s + a_{i1}}\widetilde{V}_{i-1}. \tag{A.10}$$

Considering that $\widetilde{V}_0 = \widetilde{V}_{\mathrm{H}}$, we express each $\widetilde{V}_i$ from $\widetilde{V}_{\mathrm{H}}$ as:

$$\widetilde{V}_i = \Omega_i \widetilde{V}_{\mathrm{H}}, \tag{A.11}$$

with $\Omega_i = \prod_{j=1}^{i} \frac{a_{j3}s + a_{j1}}{s^2 + a_{j2}s + a_{j1}}$. Note that $\Omega_i = P_i/P_0$ based on (24).

For the head CAV, we have the Laplace transform of the linearized dynamics (A.3)–(A.4) as:

$$s\widetilde{S}_{\mathrm{H}} = \widetilde{V}_{\mathrm{d}} - \widetilde{V}_{\mathrm{H}}, \tag{A.12}$$

$$s\widetilde{V}_{\mathrm{H}} = \xi_{\mathrm{H}}\widetilde{S}_{\mathrm{H}} - \eta_{\mathrm{H}}\widetilde{V}_{\mathrm{H}} + \beta_{\mathrm{H,d}}\widetilde{V}_{\mathrm{d}} + \sum_{i\in\mathcal{N}_{\mathrm{H}}} \beta_{\mathrm{H},i}\widetilde{V}_i + \beta_{\mathrm{H,T}}\widetilde{V}_{\mathrm{T}}, \tag{A.13}$$

which gives:

$$\widetilde{V}_{\mathrm{H}} = \frac{(\beta_{\mathrm{H,d}}s + \xi_{\mathrm{H}})\widetilde{V}_{\mathrm{d}} + \beta_{\mathrm{H,T}}s\widetilde{V}_{\mathrm{T}} + \sum_{i\in\mathcal{N}_{\mathrm{H}}} \beta_{\mathrm{H},i}s\widetilde{V}_i}{s^2 + \eta_{\mathrm{H}}s + \xi_{\mathrm{H}}}. \tag{A.14}$$

By substituting $\widetilde{V}_i$ from (A.11), we obtain:

$$\widetilde{V}_{\mathrm{H}} = \frac{(\beta_{\mathrm{H,d}}s + \xi_{\mathrm{H}})\widetilde{V}_{\mathrm{d}} + \beta_{\mathrm{H,T}}s\widetilde{V}_{\mathrm{T}}}{s^2 + \eta_{\mathrm{H}}s + \xi_{\mathrm{H}} - \sum_{i\in\mathcal{N}_{\mathrm{H}}} \beta_{\mathrm{H},i}s\Omega_i}. \tag{A.15}$$

For the tail CAV, taking the Laplace transform of the linearized dynamics (A.5)–(A.6) leads to:

$$s\widetilde{S}_{\mathrm{T}} = \widetilde{V}_{\mathrm{N}} - \widetilde{V}_{\mathrm{T}}, \tag{A.16}$$

$$s\widetilde{V}_{\mathrm{T}} = \xi_{\mathrm{T}}\widetilde{S}_{\mathrm{T}} - \eta_{\mathrm{T}}\widetilde{V}_{\mathrm{T}} + \beta_{\mathrm{T,N}}\widetilde{V}_{\mathrm{N}} + \sum_{i\in\mathcal{N}_{\mathrm{T}}} \beta_{\mathrm{T},i}\widetilde{V}_i + \beta_{\mathrm{T,H}}\widetilde{V}_{\mathrm{H}}, \tag{A.17}$$

which gives:

$$\widetilde{V}_{\mathrm{T}} = \frac{\beta_{\mathrm{T,H}}s\widetilde{V}_{\mathrm{H}} + (\beta_{\mathrm{T,N}}s + \xi_{\mathrm{T}})\widetilde{V}_{\mathrm{N}} + \sum_{i\in\mathcal{N}_{\mathrm{T}}} \beta_{\mathrm{T},i}s\widetilde{V}_i}{s^2 + \eta_{\mathrm{T}}s + \xi_{\mathrm{T}}}. \tag{A.18}$$

By substituting $\widetilde{V}_i$ from (A.11), we get:

$$\widetilde{V}_{\mathrm{H}} = \frac{(s^2 + \eta_{\mathrm{T}}s + \xi_{\mathrm{T}})\widetilde{V}_{\mathrm{T}}}{\beta_{\mathrm{T,H}}s + (\beta_{\mathrm{T,N}}s + \xi_{\mathrm{T}})\Omega_{\mathrm{N}} + \sum_{i\in\mathcal{N}_{\mathrm{T}}} \beta_{\mathrm{T},i}s\Omega_i}. \tag{A.19}$$

Equation (A.15) and (A.19) leads to:

$$\frac{(\beta_{\mathrm{H,d}}s + \xi_{\mathrm{H}})\widetilde{V}_{\mathrm{d}} + \beta_{\mathrm{H,T}}s\widetilde{V}_{\mathrm{T}}}{s^2 + \eta_{\mathrm{H}}s + \xi_{\mathrm{H}} - \sum_{i\in\mathcal{N}_{\mathrm{H}}} \beta_{\mathrm{H},i}s\Omega_i} = \frac{(s^2 + \eta_{\mathrm{T}}s + \xi_{\mathrm{T}})\widetilde{V}_{\mathrm{T}}}{\beta_{\mathrm{T,H}}s + (\beta_{\mathrm{T,N}}s + \xi_{\mathrm{T}})\Omega_{\mathrm{N}} + \sum_{i\in\mathcal{N}_{\mathrm{T}}} \beta_{\mathrm{T},i}s\Omega_i}. \tag{A.20}$$

This can be rearranged to obtain the head-to-tail transfer function defined in (20):

$$G(s) = \frac{(\beta_{\mathrm{H,d}}s + \xi_{\mathrm{H}})(\beta_{\mathrm{T,H}}s + (\beta_{\mathrm{T,N}}s + \xi_{\mathrm{T}})\Omega_{\mathrm{N}} + \sum_{i\in\mathcal{N}_{\mathrm{T}}} \beta_{\mathrm{T},i}s\Omega_i)}{\left(s^2 + \eta_{\mathrm{H}}s + \xi_{\mathrm{H}} - \sum_{i\in\mathcal{N}_{\mathrm{H}}} \beta_{\mathrm{H},i}s\Omega_i\right)(s^2 + \eta_{\mathrm{T}}s + \xi_{\mathrm{T}}) - \beta_{\mathrm{H,T}}s(\beta_{\mathrm{T,H}}s + (\beta_{\mathrm{T,N}}s + \xi_{\mathrm{T}})\Omega_{\mathrm{N}} + \sum_{i\in\mathcal{N}_{\mathrm{T}}} \beta_{\mathrm{T},i}s\Omega_i)}. \tag{A.21}$$

Since $\Omega_i = P_i/P_0$ based on (24), we multiply both the numerator and denominator by P_0, and we get (21)–(23).

y 11

Appendix B. Safety Analysis

In this Appendix, we first prove Theorem 2 that provides safe controller gains for the nominal controller in Section 4. Then, we establish robust CBF constraints for HV safety, which are utilized in (72) in Section 6.

B.1. Proof of Theorem 2

Proof. We prove safety based on Lemma 1, by showing that $\dot{h}_{\mathrm{H}}(\mathbf{x}, v_{\mathrm{d}}) \geq 0$ holds if $h_{\mathrm{H}}(\mathbf{x}) = 0$. We express $\dot{h}_{\mathrm{H}}(\mathbf{x}, v_{\mathrm{d}})$:

$$\dot{h}_{\mathrm{H}}(\mathbf{x}, v_{\mathrm{d}}) = v_{\mathrm{d}} - v_{\mathrm{H}} - \tau_{\mathrm{H}}u_{\mathrm{H}}, \tag{B.1}$$

where we substitute the nominal controller $u_{\mathrm{H}} = k_{\mathrm{H,n}}(\mathbf{x}, v_{\mathrm{d}})$ from (12):

$$\dot{h}_{\mathrm{H}}(\mathbf{x}, v_{\mathrm{d}}) = v_{\mathrm{d}} - v_{\mathrm{H}} - \tau_{\mathrm{H}}\left(\alpha_{\mathrm{H}}(V_{\mathrm{H}}(s_{\mathrm{H}}) - v_{\mathrm{H}}) + \beta_{\mathrm{H,d}}(W(v_{\mathrm{d}}) - v_{\mathrm{H}}) + \sum_{i\in\mathcal{N}_{\mathrm{H}}} \beta_{\mathrm{H},i}(W(v_i) - v_{\mathrm{H}}) + \beta_{\mathrm{H,T}}(W(v_{\mathrm{T}}) - v_{\mathrm{H}})\right). \tag{B.2}$$

Then, we consider $v_{\mathrm{d}}, v_{\mathrm{H}}, v_i, v_{\mathrm{T}} \in [0, v_{\max}]$, $s_{\mathrm{H}} \in [s_{\mathrm{st}}, s_{\mathrm{go}}]$, and we substitute W and V_{H} from (13) and (15):

$$\dot{h}_{\mathrm{H}}(\mathbf{x}, v_{\mathrm{d}}) = v_{\mathrm{d}} - v_{\mathrm{H}} - \tau_{\mathrm{H}}\left(\alpha_{\mathrm{H}}\left(\kappa(s_{\mathrm{H}} - s_{\mathrm{st}}) - v_{\mathrm{H}}\right) + \beta_{\mathrm{H,d}}(v_{\mathrm{d}} - v_{\mathrm{H}}) + \sum_{i\in\mathcal{N}_{\mathrm{H}}} \beta_{\mathrm{H},i}(v_i - v_{\mathrm{H}}) + \beta_{\mathrm{H,T}}(v_{\mathrm{T}} - v_{\mathrm{H}})\right). \tag{B.3}$$

Next, we rearrange the terms and consider $h_{\mathrm{H}}(\mathbf{x}) = 0$, that is, $s_{\mathrm{H}} = \tau_{\mathrm{H}}v_{\mathrm{H}}$:

$$\dot{h}_{\mathrm{H}}(\mathbf{x}, v_{\mathrm{d}}) = (1 - \tau_{\mathrm{H}}\beta_{\mathrm{H,d}})(v_{\mathrm{d}} - v_{\mathrm{H}}) - \alpha_{\mathrm{H}}\left(\kappa\tau_{\mathrm{H}}(s_{\mathrm{H}} - s_{\mathrm{st}}) - s_{\mathrm{H}}\right) - \tau_{\mathrm{H}}\left(\sum_{i\in\mathcal{N}_{\mathrm{H}}} \beta_{\mathrm{H},i}(v_i - v_{\mathrm{H}}) + \beta_{\mathrm{H,T}}(v_{\mathrm{T}} - v_{\mathrm{H}})\right). \tag{B.4}$$

Since $v_{\mathrm{d}}, v_{\mathrm{H}}, v_i, v_{\mathrm{T}} \in [0, v_{\max}]$, we have $|v_{\mathrm{d}} - v_{\mathrm{H}}| \leq v_{\max}$, $|v_i - v_{\mathrm{H}}| \leq v_{\max}$, and $|v_{\mathrm{T}} - v_{\mathrm{H}}| \leq v_{\max}$. Furthermore, since $s_{\mathrm{H}} \in [s_{\mathrm{st}}, s_{\mathrm{go}}]$ and $\kappa \leq 1/\tau_{\mathrm{H}}$, we have $\kappa\tau_{\mathrm{H}}(s_{\mathrm{H}} - s_{\mathrm{st}}) - s_{\mathrm{H}} \leq -s_{\mathrm{st}}$. Substituting these and using $\alpha_{\mathrm{H}} \geq 0$ leads to:

$$\dot{h}_{\mathrm{H}}(\mathbf{x}, v_{\mathrm{d}}) \geq -|1 - \tau_{\mathrm{H}}\beta_{\mathrm{H,d}}|v_{\max} + \alpha_{\mathrm{H}}s_{\mathrm{st}} - \tau_{\mathrm{H}}\left(\sum_{i\in\mathcal{N}_{\mathrm{H}}} |\beta_{\mathrm{H},i}| + |\beta_{\mathrm{H,T}}|\right)v_{\max}. \tag{B.5}$$

Finally, substituting (40) leads to $\dot{h}_{\mathrm{H}}(\mathbf{x}, v_{\mathrm{d}}) \geq 0$ which completes the proof. □

B.2. Robust CBF constraints for HV safety

Finally, we discuss how the head CAV's controller may ensure HV safety when the human driver model is inaccurate, which is captured by nonzero disturbance $\mathbf{d} \neq 0$ in (3) and $d_i \neq 0$ in (5). To this end, we briefly discuss robust safety-critical control for systems with disturbance, based on robust CBF theory Jankovic (2018).

Consider system (45) with an additive disturbance $\mathbf{d} \in D \subset \mathbb{R}^n$:

$$\dot{\mathbf{x}} = f(\mathbf{x}) + g(\mathbf{x})\mathbf{u} + \mathbf{d}, \tag{B.6}$$

cf. (3). Analogously to (47) in Theorem 4, it can be stated that controllers $\mathbf{u} = k(\mathbf{x})$ satisfying:

$$L_f h(\mathbf{x}) + L_g h(\mathbf{x})k(\mathbf{x}) + \nabla h(\mathbf{x}) \cdot \mathbf{d} \geq -\gamma(h(\mathbf{x})), \quad \forall \mathbf{x} \in C, \quad \forall \mathbf{d} \in D, \tag{B.7}$$

render the set C forward invariant (safe) for the corresponding closed-loop system with disturbance. The difficulty of satisfying this constraint is that the disturbance $\mathbf{d}$ may be unknown. However, if the disturbance has a known bound $\bar{\mathbf{d}} > 0$, that is, if $\|\mathbf{d}\|_\infty \leq \bar{\mathbf{d}}$ holds, then robust CBF theory provides the following sufficient condition for a safe controller Jankovic (2018):

$$L_f h(\mathbf{x}) + L_g h(\mathbf{x})k(\mathbf{x}) - \|\nabla h(\mathbf{x})\|\bar{\mathbf{d}} \geq -\gamma(h(\mathbf{x})), \quad \forall \mathbf{x} \in C, \tag{B.8}$$

which implies that (B.7) holds.

In the context of guaranteeing HV safety, the following modification of (58) can be used as robust CBF constraint.

Theorem 5 (Robust HV safety with bounded HV model error)**.** *Consider system (3) with disturbance given in (10). Assume that there is a known bound $\bar{d}_i \in \mathbb{R}$ for the disturbance d_i, i.e., $|d_i| \leq \bar{d}_i$. If the controller of the head CAV satisfies (51) and:*

$$L_f \bar{h}_i(\mathbf{x}, v_{\mathrm{d}}) + L_{g_{\mathrm{H}}} \bar{h}_i(\mathbf{x})u_{\mathrm{H}} - \tau_i\bar{d}_i \geq -\gamma_i \bar{h}_i(\mathbf{x}), \tag{B.9}$$

with $\gamma_i > 0$ and $\bar{h}_i$ defined in (57), then HV-i is safe w.r.t. the CTH policy defined in (37).

Proof. Considering the system (3) and (10) with the safety function $\bar{h}_i$ in (57), the CBF constraint corresponding to (B.7) is:

$$L_f \bar{h}_i(\mathbf{x}, v_\mathrm{d}) + L_{g_\mathrm{H}} \bar{h}_i(\mathbf{x}) u_\mathrm{H} + \frac{\partial \bar{h}_i}{\partial v_i} d_i \geq -\gamma_i \bar{h}_i(\mathbf{x}), \tag{B.10}$$

where $\frac{\partial \bar{h}_i}{\partial v_i} = -\tau_i$. Since the disturbance d_i is upper bounded by $\bar{d}_i$, we have $\frac{\partial \bar{h}_i}{\partial v_i} d_i \geq -\tau_i \bar{d}_i$. Therefore, (B.9) implies (B.10) and leads to a sufficient condition for guaranteeing safety w.r.t. $\bar{h}_i$, analogously to (B.8). Furthermore, (51) ensures safety w.r.t. h_H defined in (34). Based on (57), ensuring both $h_\mathrm{H}(\mathbf{x}) \geq 0$ and $\bar{h}_i(\mathbf{x}) \geq 0$ implies $h_i(\mathbf{x}) \geq 0$, which means safety w.r.t. the CTH policy defined in (37). □

Remark 11 (Effect of HV model error on safety constraints)**.** Compared with the HV safety constraint (58), the robust HV safety constraint (B.9) has an extra safety margin term $\tau_i \bar{d}_i$, which accounts for the human model error. The safety margin is proportional to the model error $\bar{d}_i$, which means a less accurate human driver model will cause a more aggressive control strategy. Specifically, when $\bar{d}_i = 0$, the robust safety constraint (B.9) becomes the same as the original safety constraint (58).

References

Alan, A., He, T. G. C.R., Molnar, J.C., Mathew, H., Bell, G., Orosz, 2024. Integrating safety with performance in connected automated truck control: experimental validation. IEEE Trans. Intell. Veh. 9 (1), 3075–3088.

Althoff, M., Dolan, J.M., 2014. Online verification of automated road vehicles using reachability analysis. IEEE Trans. Rob. 30 (4), 903–918.

Ames, J. W. A.D., Grizzle, P., Tabuada, 2014. Control barrier function based quadratic programs with application to adaptive cruise control. In: 53Rd IEEE Conference on Decision and Control. IEEE, pp. 6271–6278.

Ames, S. A.D., Coogan, M., Egerstedt, G., Notomista, K., Sreenath, P., Tabuada, 2019. Control barrier functions: theory and applications. In: 18Th European Control Conference. IEEE, pp. 3420–3431.

Bai, W., Xu, B., Liu, H., Qin, Y., Xiang, C., 2022a. Robust longitudinal distributed model predictive control of connected and automated vehicles with coupled safety constraints. IEEE Trans. Veh. Technol. 72 (3), 2960–2973.

Bai, Z., Hao, P., Shangguan, W., Cai, B., Barth, M.J., 2022b. Hybrid reinforcement learning-based eco-driving strategy for connected and automated vehicles at signalized intersections. IEEE Trans. Intell. Transp. Syst. 23 (9), 15850–15863.

Bando, M., Hasebe, K., Nakanishi, K., Nakayama, A., 1998. Analysis of optimal velocity model with explicit delay. Phys. Rev. E 58 (5), 5429–5435.

Bekiaris-Liberis, N., 2023. Robust string stability and safety of cth predictor-feedback cacc. IEEE Trans. Intell. Transp. Syst. 24 (8), 8209–8221.

Brunner, J.S., Makridis, M. A., Kouvelas, A., 2022. Comparing the observable response times of acc and cacc systems. IEEE Trans. Intell. Transp. Syst. 23 (10), 19299–19308.

Chaozhe, R., He, G., Orosz, 2018. Safety guaranteed connected cruise control. In: 21St International Conference on Intelligent Transportation Systems, pp. 549–554.

Chen, X., Lin, X., Li, M., 2023. Fang he, and qiang meng. a nearly throughput-maximum knotted intersection design and control for connected and automated vehicles. Transp. Res. Part B: Methodol. 171, 44–79.

Dai, Y., Yang, Y., Wang, Z., Luo, Y., 2022. Exploring the impact of damping on connected and autonomous vehicle platoon safety with cacc. Physica A 607, 128181.

Dey, L. K.C., Yan, X., Wang, Y., Wang, H., Shen, M., Chowdhury, L., Yu, C., Qiu, V., Soundararaj, 2015. A review of communication, driver characteristics, and controls aspects of cooperative adaptive cruise control (cacc). IEEE Trans. Intell. Transp. Syst. 17 (2), 491–509.

Ding, J., Peng, H., Zhang, Y., Li, L., 2020. Penetration effect of connected and automated vehicles on cooperative on-ramp merging. IET Intel. Transport Syst. 14 (1), 56–64.

Do, W., Omid, M.R., Miranda-Moreno, L., et al. 2019. Simulation-based connected and automated vehicle models on highway sections: a literature review. p. 9343705.

Fhwa, 2007. Next Generation Simulation (NGSIM).

Garg, M., Bouroche, M., 2023. Can connected autonomous vehicles improve mixed traffic safety without compromising efficiency in realistic scenarios? IEEE Trans. Intell. Transp. Syst. 24 (6), 6674–6689.

Ge, J., Avedisov, S.S., He, C.R., Qin, M. W.B., Sadeghpour, G., Orosz, 2018. Experimental validation of connected automated vehicle design among human-driven vehicles. Transp. Res. Part C: Emerg. Technol. 91, 335–352.

Giammarino, V., Baldi, S., Frasca, P., Monache, M. L.D., 2020. Traffic flow on a ring with a single autonomous vehicle: an interconnected stability perspective. IEEE Trans. Intell. Transp. Syst. 22 (8), 4998–5008.

Gong, S., Du, L., 2018. Cooperative platoon control for a mixed traffic flow including human drive vehicles and connected and autonomous vehicles. Transp. Res. Part B: Methodol. 116, 25–61.

Gunter, G., Gloudemans, D., Stern, S. R.E., Mcquade, R., Bhadani, M., Bunting, M., Monache, L.D., Lysecky, R., Seibold, B., 2020. Are commercially implemented adaptive cruise control systems string stable? IEEE Trans. Intell. Transp. Syst. 22 (11), 6992–7003.

Guo, S., Orosz, G., Molnar, T.G., 2023. Connected cruise and traffic control for pairs of connected automated vehicles. IEEE Trans. Intell. Transp. Syst. 24 (11), 12648–12658.

Han, X., Ma, R., Michael, H., Zhang, 2020. Energy-aware trajectory optimization of cav platoons through a signalized intersection. Transp. Res. Part C: Emerg. Technol. 118, 102652.

Jankovic, M., 2018. Robust control barrier functions for constrained stabilization of nonlinear systems. Automatica 96, 359–367.

Jin, L., Čičić, M., Johansson, K.H., Amin, S., 2020. Analysis and design of vehicle platooning operations on mixed-traffic highways. IEEE Trans. Automat. Contr. 66 (10), 4715–4730.

Johansson, A., Bai, T., Johansson, K.H., Mårtensson, J., 2023. Platoon cooperation across carriers: from system architecture to coordination. IEEE Intell. Transp. Syst. Mag. 15 (3), 132–144.

Kim, Y., Guanetti, J., Borrelli, F., 2021. Compact cooperative adaptive cruise control for energy saving: air drag modelling and simulation. IEEE Trans. Veh. Technol. 70 (10), 9838–9848.

Kuutti, S., Fallah, S., Katsaros, K., Dianati, M., Mccullough, F., Mouzakitis, A., 2018. A survey of the state-of-the-art localization techniques and their potentials for autonomous vehicle applications. IEEE Internet Things J. 5 (2), 829–846.

Li, X., 2022. Trade-off between safety, mobility and stability in automated vehicle following control: an analytical method. Transp. Res. Part B: Methodol. 166, 1–18.

Liu, H., Lu, X.-Y., Shladover, S.E., 2020. Mobility and energy consumption impacts of cooperative adaptive cruise control vehicle strings on freeway corridors. Transp. Res. Rec. 2674 (9), 111–123.

Molnar, T.G., Orosz, G., Ames, A.D., 2023. On the safety of connected cruise control: analysis and synthesis with control barrier functions. In: 62Nd IEEE Conference on Decision and Control. IEEE, pp. 1106–1111.

Nagumo, M., 1942. Über die lage der integralkurven gewöhnlicher differentialgleichungen. Proc. Physico-Math. Soc. Japan. 3rd Ser. 24, 551–559.

Orosz, G., 2016. Connected cruise control: modelling, delay effects, and nonlinear behaviour. Veh. Syst. Dyn. 54 (8), 1147–1176.

Papadoulis, A., Quddus, M., Imprialou, M., 2019. Evaluating the safety impact of connected and autonomous vehicles on motorways. Accident Anal. Prevent. 124, 12–22.

Qiu, J., Du, L., 2023. Cooperative trajectory control for synchronizing the movement of two connected and autonomous vehicles separated in a mixed traffic flow. Transp. Res. Part B: Methodol. 174, 102769.

Rios-Torres, J., Malikopoulos, A.A., 2016. Automated and cooperative vehicle merging at highway on-ramps. IEEE Trans. Intell. Transp. Syst. 18 (4), 780–789.

Seyedeh, M., Mousavi, Osama, A., Osman, D., Lord, K.K., Dixon, B., Dadashova, 2021. Investigating the safety and operational benefits of mixed traffic environments with different automated vehicle market penetration rates in the proximity of a driveway on an urban arterial. Accident Anal. Prevent. 152, 105982.
Shi, H., Zhou, Y., Wu, K., Wang, X., Lin, Y., Ran, B., . Connected automated vehicle cooperative control with a deep reinforcement learning approach in a mixed traffic environment. Transp. Res. Part C: Emerg. Technol. 133, 2021, 103421.
Shladover, D. S.E., Su, X.-Y., Lu, 2012. Impacts of cooperative adaptive cruise control on freeway traffic flow. Transp. Res. Rec. 2324 (1), 63–70.
Stern, R.E., Cui, S., Monache, M.L.D., Bhadani, R., Bunting, M., Churchill, M., Hamilton, N., Pohlmann, H., Wu, F., Piccoli, B., et al. 2018. Dissipation of stop-and-go waves via control of autonomous vehicles: field experiments. Transp. Res. Part C: Emerg. Technol. 89, 205–221.
Talebpour, A., Mahmassani, H.S., 2016. Influence of connected and autonomous vehicles on traffic flow stability and throughput. Transp. Res. Part C: Emerg. Technol. 71, 143–163.
Treiber, M., Hennecke, A., Helbing, D., 2000. Congested traffic states in empirical observations and microscopic simulations. Phys. Rev. E 62, 1805–1824.
Vaio, M.D., Fiengo, G., Petrillo, A., Salvi, A., Santini, S., Tufo, M., 2019. Cooperative shock waves mitigation in mixed traffic flow environment. IEEE Trans. Intell. Transp. Syst. 20 (12), 4339–4353.
Wang, C., Xie, Y., Huang, H., Liu, P., 2021. A review of surrogate safety measures and their applications in connected and automated vehicles safety modeling. Accident Anal. Prevent. 157, 106157.
Wang, J., Zheng, Y., Chen, C., Xu, Q., Li, K., 2022. Leading cruise control in mixed traffic flow: system modeling, controllability, and string stability. IEEE Trans. Intell. Transp. Syst. 23 (8), 12861–12876.
Wang, J., Zhou, A., Liu, Z., Peeta, S., 2024. Robust cooperative control strategy for a platoon of connected and autonomous vehicles against sensor errors and control errors simultaneously in a real-world driving environment. Transp. Res. Part B: Methodol. 184, 102946.
Wang, Z., Wu, G., Barth, M., 2018. Distributed consensus-based cooperative highway on-ramp merging using V2X communications. Technical Report. Technical report.
Xiao, W., Cassandras, C.G., Belta, C.A., 2021. Bridging the gap between optimal trajectory planning and safety-critical control with applications to autonomous vehicles. Automatica 129, 109592.
Ye, L., Yamamoto, T., 2019. Evaluating the impact of connected and autonomous vehicles on traffic safety. Physica A 526, 121009.
Yi, Z., Li, L., Qu, X., Hong, Y., Mao, P., Ran, B., 2020. Using artificial potential field theory for a cooperative control model in a connected and automated vehicles environment. Transp. Res. Rec. 2674 (9), 1005–1018.
Yu, H., Koga, S., Krstic, M., 2018. Stabilization of traffic flow with a leading autonomous vehicle. Vol. 51906. American Society of Mechanical Engineers.
Zhang, H., Du, L., Shen, J., 2022. Hybrid mpc system for platoon based cooperative lane change control using machine learning aided distributed optimization. Transp. Res. Part B: Methodol. 159, 104–142.
Zhao, C., Molnar, T.G., Yu, H., 2024. Safety-critical stabilization of mixed traffic by pairs of cavs. In: 2024 American Control Conference. IEEE, pp. 743–748.
Zhao, C., Yu, H., Molnar, T.G., 2023. Safety-critical traffic control by connected automated vehicles. Transp. Res. Part C: Emerg. Technol. 154, 104230.
Zhao, T., Yurtsever, E., Paulson, J.A., Rizzoni, G., 2022. Formal certification methods for automated vehicle safety assessment. IEEE Trans. Intell. Veh. 8 (1), 232–249.
Zheng, Y., Ran, B., Qu, X., Zhang, J., Lin, Y., 2019. Cooperative lane changing strategies to improve traffic operation and safety nearby freeway off-ramps in a connected and automated vehicles environment. IEEE Trans. Intell. Transp. Syst. 21 (11), 4605–4614.
Zhou, J., Zhu, F., 2021. Analytical analysis of the effect of maximum platoon size of connected and automated vehicles. Transp. Res. Part C: Emerg. Technol. 122, 102882.
Zhou, Y., Zhong, X., Chen, Q., Ahn, S., Jiang, J., Jafarsalehi, G., 2023a. Data-driven analysis for disturbance amplification in car-following behavior of automated vehicles. Transp. Res. Part B: Methodol. 174, 102768.
Zhou, Z., Li, L., Qu, X., Ran, B., 2023b. An autonomous platoon formation strategy to optimize cav car-following stability under periodic disturbance. Physica A 626, 129096.